10

Rapid #: -1425040

Ariel IP: 128.187.72.80

CALL #:	**QC1 .I6780**
LOCATION:	**NED :: Snell Library :: sp**
TYPE:	Article CC:CCL
JOURNAL TITLE:	International journal of mass spectrometry and ion processes
USER JOURNAL TITLE:	International Journal of Mass Spectrometry and Ion Processes
NED CATALOG TITLE:	International journal of mass spectrometry and ion processes.
ARTICLE TITLE:	I don't know the title
ARTICLE AUTHOR:	Guan, S. and Marshall, A. G.
VOLUME:	157/158
ISSUE:	
MONTH:	
YEAR:	1996
PAGES:	5-37 OK PD
ISSN:	0168-1176
OCLC #:	
CROSS REFERENCE ID:	1042955
VERIFIED:	

BORROWER:	**UBY :: Main Library**
PATRON:	**Hart,Grant**
PATRON ID:	
PATRON ADDRESS:	
PATRON PHONE:	
PATRON FAX:	
PATRON E-MAIL:	grant_hart@byu.edu
PATRON DEPT:	Physics and Astronomy
PATRON STATUS:	Faculty/Admin
PATRON NOTES:	

ELSEVIER

International Journal of Mass Spectrometry and Ion Processes 157/158 (1996) 5–37

International Journal of Mass Spectrometry and Ion Processes

Stored waveform inverse Fourier transform (SWIFT) ion excitation in trapped-ion mass spectometry: theory and applications

Shenheng Guan*, Alan G. Marshall

Center for Interdisciplinary Magnetic Resonance, National High Magnetic Field Laboratory, Department of Chemistry, Florida State University, 1800 E. Paul Dirac Drive, Tallahassee, FL 32310, USA

Received 11 April 1996; accepted 23 July 1996

Abstract

Stored waveform excitation produced by inverse Fourier transformation of a specified magnitude/phase excitation spectrum offers the most general and versatile means for broadband mass-selective excitation and ejection in Penning (FT-ICR) and Paul (quadrupole) ion trap mass spectrometry. Since the last comprehensive review of SWIFT excitation in 1987, the technique has been adopted, modified, and extended widely in both the ICR and quadrupole ion trap communities. Here, we review the principles, variations, algorithms, hardware implementation, and some applications of SWIFT for both ICR and quadrupole ion trap mass spectrometry.

We show that the most desirable SWIFT waveform is that optimized to reduce both the time-domain SWIFT maximum amplitude and the amplitude near the start and end of the SWIFT waveform. We examine the "true" magnitude excitation spectrum, obtained by zero-filling and forward Fourier transforming the SWIFT time-domain waveform, in order to evaluate the trade-off between spectral magnitude uniformity and frequency (mass) selectivity. Apodization of the SWIFT waveform is optimally conducted by smoothing the excitation magnitude spectrum prior to generation of the SWIFT waveform by inverse FT. When (as for broadband ejection in a quadrupole ion trap) it is important that ions be excited near-simultaneously over a wide mass range, the phase spectrum (before inverse FT to generate the SWIFT waveform) may be overmodulated or randomly modulated ("filtered noise field"), with the recognition that very substantial non-uniformity in the "true" excitation magnitude spectrum will result.

Keywords: Ion cyclotron resonance; Excitation methods; Trapped ion mass spectra

1. Introduction

Fourier transform nuclear magnetic resonance (FT-NMR) spectroscopy and Fourier transform ion cyclotron resonance (FT-ICR) mass spectrometry (also known as FT-MS) are based on pulsed excitation to generate coherent (and therefore detectable) motion of ensembles of spins (NMR) or ions (ICR) [1]. In either type of spectroscopy, the versatility of the experiment derives from its ability to select and manipulate spins (ions) of different resonant Larmor (cyclotron) frequency by frequency-selective excitation. For example, "shaped" frequency-selective pulses [2] facilitate such desirable NMR techniques as solvent suppression (to improve dynamic range), selective decoupling or cross-polarization (for establishing through-bond or through-space couplings), and slice selection (in magnetic resonance imaging). In

* Corresponding author.

PII S0168-1176(96)04461-8

FT-ICR mass spectrometry, frequency-selective excitation makes it possible to detect, remeasure, heat (to induce reaction or fragmentation), or even remove from the spectrometer ions of selected mass-to-charge ratios. Frequency "encodement" may also be achieved by multiple-excitation event sequences, such as early two-dimensional FT-ICR mass spectrometry [3,4].

Because of the many conceptual similarities shared by nuclear magnetic resonance (NMR) and ICR spectroscopies, various techniques have developed in parallel in both communities [1]. In particular, stored-waveform inverse Fourier transform (SWIFT) excitation, which forms the subject of this review, was inspired by "tailored" broadband selective excitation developed much earlier in NMR for solvent suppression [5], although excitation and detection were time-shared rather than time-sequential in the NMR experiment. It is also fair to note some major differences in excitation requirements for NMR and ICR. First, excitation bandwidth in ICR can be three orders of magnitude broader (i.e., from kHz to MHz) than that for routine high-resolution NMR. Second, although ion cyclotron resonances are typically more sparsely distributed than in NMR spectra, frequency selectivity requirements can also be very high in ICR since motion of trapped ions of different mass-to-charge ratios is essentially decoupled from each other and from the environment. Third, ICR response is linearly proportional to excitation (see below), whereas NMR is linear only for very small excitation amplitude [1]. The combination of wide bandwidth and high frequency selectivity have driven the development of ICR excitation in different directions from that of NMR.

In this review, we provide a comprehensive treatment of ion cyclotron excitation methods in FT-ICR mass spectrometry. We begin by describing the three "natural" ICR motional trajectories (cyclotron rotation, magnetron rotation, and axial oscillation) in an applied uniform static magnetic field and quadrupolar axial electrostatic "trapping" potential, and how they are affected by an oscillating dipolar electric excitation potential. The theoretical (and, to a very good approximation, the experimental) linearity of ICR excitation/detection has two important consequences: (a) Ion motional amplitude is proportional to excitation amplitude at the ion cyclotron frequency, and (b) the principle of superposition makes it possible to compute the signal from many ions simply by adding the signals from individual ions. Linear response theory makes it possible to: (a) find the post-excitation ion cyclotron radius without solving the equation of ion motion directly; and (b) obtain the ion response to complex excitation waveforms whose ion trajectories do not have analytical solutions. (Linear response theory also applies to resonant excitation in an r.f. quadrupole ion trap, and (in the small tip-angle limit) to excitation in a two-energy level NMR spin system.) We then proceed to analyze each of several common FT-ICR excitation waveforms, based on a common theoretical foundation: single-frequency, frequency-sweep ("chirp"), and impulse. We also derive and describe ion trajectories for three popular ion activation methods: multiple excitation collision activation (MECA) [6], very-low-energy (VLE) excitation [7–9], and sustained off-resonance irradiation (SORI) [10]. Stored-waveform inverse Fourier transform (SWIFT) algorithms and their practical implementation are reviewed for the first time since 1987 [11]. Finally, we also establish a rigorous relation between multi-segment spectral smoothing and time-domain waveform amplitude, so as to produce optimally frequency-selective excitation with optimally low time-domain dynamic range.

2. The FT-ICR experiment

FT-ICR MS offers ultrahigh mass resolving power, multistage MST in a single mass

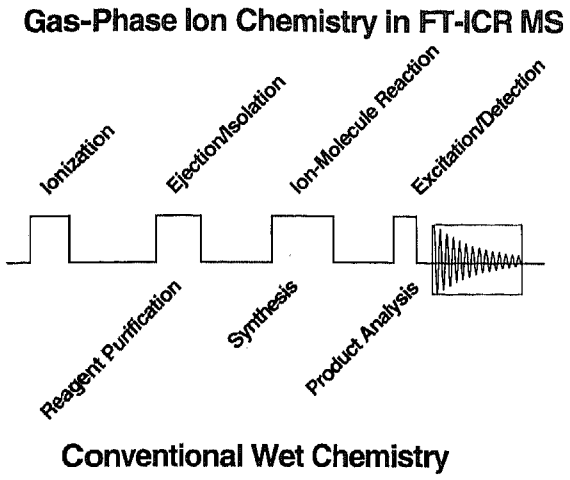

Fig. 1. Comparison of ion–molecule reactions conducted in the gas-phase and observed by FT-ICR mass spectrometry (top) vs. condensed-phase conventional "wet" chemistry (bottom). Note the one-to-one correspondence in each step between gas-phase and solution-phase chemistry.

analyzer, wide mass range, simultaneous detection of all ions, and long ion storage period. With these capabilities, an FT-ICR mass spectrometer may be thought of as a complete chemical laboratory for gas-phase Ions. Fig. 1 compares gas-phase ion–molecule reactions with conventional condensed-phase "wet" chemistry: FT-ICR makes it possible to perform the usual wet-chemical processes (reagent purification, synthesis, product analysis) in the gas-phase, with three important differences. First, the series of steps shown in Fig. 1 can typically be completed in the gas-phase in a few seconds or minutes, compared to hours or days in condensed phase. Second, the gas-phase steps are conducted in the absence of solvent, whose presence in condensed-phase experiments can strongly affect the reaction (by differential solvation of reactants and products, or even direct reaction with reactants or products). Third, ions may easily be heated to energies of 1–100 eV, to reach an effective "temperature" of up to approximately 10^6 K for investigation of endothermic and/or fragmentation reactions.

In the gas-phase FT-ICR experiment, ions are generated in or injected into an ICR (Penning) ion trap. Ions of given mass-to-charge ratio(s) of interest may then be isolated by radial ejection from the trap of ions of all other mass-to-charge ratios. The ions remaining in the trap may then be allowed to react with neutral molecules, and the product ions mass analyzed.

Excitation of ion cyclotron motion is a central aspect of all FT-ICR experiments. Excitation provides for simple and rapid ion isolation and activation, and the same theoretical analysis applies to ion detection as well. Virtually all FT-ICR experiments are conducted in a "Penning" ICR ion trap: namely, ions are confined within a spatial volume of a few cm^3 by the combination of a strong static spatially uniform magnetic field and a quadrupolar axial electrostatic "trapping" potential. Ion trajectories in such a trap may be analyzed into three independent "natural" motions: cyclotron rotation, magnetron rotation, and axial oscillation between the two "end caps" of the trap [12].The three ion motions may be treated as harmonic oscillators with very different dependences of motional frequency on ion mass-to-charge ratio.

$$\omega_+ = \frac{\omega_c}{2} + \sqrt{\left(\frac{\omega_c}{2}\right)^2 - \left(\frac{\omega_z^2}{2}\right)} \tag{1a}$$

$$\omega_- = \frac{\omega_c}{2} - \sqrt{\left(\frac{\omega_c}{2}\right)^2 - \left(\frac{\omega_z^2}{2}\right)} \tag{1b}$$

$$\omega_z = \sqrt{\frac{qV_{trap}}{md^2}} \tag{1c}$$

in which

$$\omega_c = \frac{qB}{m} \tag{1d}$$

is the unperturbed cyclotron frequency of an ion of mass m and charge q in a spatially homogeneous static magnetic field of amplitude B (in the negative z-direction), in the absence of any electrostatic field. V_{trap} is the trapping potential (e.g., between the trapping plates and the side plates for a cubic trap; between the ring and endcap

electrodes for a hyperbolic trap). d_0 is a measure of the trap dimensions. For a cubic trap of edge length a, for example, one finds that [13]

$$d_0^2 = \frac{a^2}{2\alpha} \qquad \alpha = 2.77373 \tag{1e}$$

ω_z, ω_- and ω_+ are the axial, magnetron, and "reduced" cyclotron frequencies. For an ion with a mass-to-charge ratio lower than the "critical" value (i.e., when

$$\left(\frac{\omega_c}{2}\right)^2 - \left(\frac{\omega_z^2}{2}\right) = 0$$

in Eqs. (1a) and (1b).

$$\nu_+ = 2\pi\omega_+ \approx \frac{A}{m/z} \tag{2a}$$

$$\nu_z = 2\pi\omega_z \approx \frac{B}{\sqrt{m/z}} \tag{2b}$$

$$\nu_- = 2\pi\omega_- \approx C \tag{2c}$$

in which A, B, and C are constants for an ion (see Fig. 2), m is ion mass in u, and z is ion charge in multiples of the elementary charge. Except at very high mass-to-charge ratio, ion magnetron frequency is nearly independent of mass-to-charge ratio; therefore, magnetron motion is not directly useful for mass measurement. On the other hand, the strong dependence of mass-to-charge ratio on ion cyclotron frequency makes ion cyclotron motion an ideal measure of mass-to-charge ratio of the ion. To measure ion cyclotron frequency, we first prepare ions near the center of the trap and excite their cyclotron motion by applying a spatially uniform and time-varying dipolar field containing components at the cyclotron frequency(ies) of ions of interest. Once excited, ion cyclotron radius increases (from a fraction of a millimeter to a centimeter or so) and ion cyclotron motion becomes spatially coherent (and thus detectable). Ions with coherent cyclotron motion induce between a pair of detection electrodes a so-called "image" current which may be converted into a voltage and then digitized and recorded [14,15].

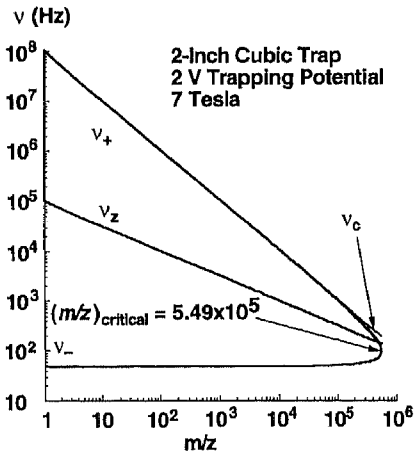

Fig. 2. Mass-to-charge ratio (m/z) dependence of the frequency of each of the three ion natural motions (cyclotron rotation, magnetron rotation, and axial oscillation) in an ICR (Penning) ion trap. At m/z values well below the "critical" m/z, the reduced cyclotron frequency, ν_+, is approximately inversely proportional to m/z, whereas axial frequency, ν_z, is approximately inversely proportional to the square root of m/z, and magnetron frequency is nearly independent of m/z. At the "critical" m/z value, $\nu_+ = \nu_- = \sqrt{2}\nu_z = \nu_c/2$. At or above the "critical" m/z value, ions are no longer trapped.

Excitation of cyclotron motion provides not only for ion detection, but also for ion isolation and activation. For example, a cyclotron excitation profile may be designed to excite only ions of selected mass-to-charge ratio(s) to cyclotron radii larger than the dimensions of the trap ("radial ejection"), without affecting ions of other mass-to-charge ratios. Such an ion isolation procedure is vital for FT-ICR tandem mass spectrometry (MS^n) in which parent ion selection and product ion detection are carried out tandem-in-time rather than tandem-in-space. Moreover, among the three natural ion motions of a given amplitude, cyclotron motion exhibits the highest kinetic energy; excitation of ion cyclotron motion is thus most effective for accelerating and activating (i.e., increasing the internal energy) of ions by collisions with neutrals to produce fragment and/or product ions. The collision-induced dissociation (CID) (also known as collision-activated dissociation, or CAD) is the most popular way to determine ion structure by FT-ICR MS [16,17].

3. Ion motion during azimuthal dipolar excitation

The approximations of spatially homogeneous static magnetic field, axial quadrupolar trapping potential, and spatially uniform dipolar (linearly polarized) azimuthal excitation electric potential in an ion trap lead to a linear equation of ion cyclotron (and magnetron) motion. We shall consider such approximated trapping and dipolar excitation potentials of the commonly used cubic trap. Ion behavior in other trap configurations has recently been reviewed [18,19]. Ion equations of cyclotron and magnetron motions during azimuthal dipolar excitation are conveniently separated by use of Brown and Gabrielse's "*V*-vector" transform [12]. The solution (namely ion trajectory) to the equations of ion motion may then be expressed as a Fourier transform integral, leading in a natural way to linear response theory.

The axial quadrupolar trapping potential approximation is important because the "natural" cyclotron, magnetron, and axial frequencies then become independent of ion location and ion motional amplitude. Spatially uniform dipolar excitation assures that the ion excitation process is independent of ion location as well. An axial quadrupolar trapping potential and uniform dipolar excitation potential have different symmetry, and are thus difficult to achieve simultaneously in a conventional ICR trap. However, we have recently proposed a "universal" trap that provides for generation of both near-perfect axial quadrupolar electrostatic trapping potential and spatially near-uniform excitation field [19].

3.1. Trapping and dipolar excitation potentials in a cubic ICR ion trap

In a cubic ICR ion trap [20], the boundary conditions at any time t for the electric potential in the trap may be written as

$$(\Phi)(x,y,z,t) = V_{x+}(t) \qquad x = +a/2 \tag{3a}$$

$$(\Phi)(x,y,z,t) = V_{x-}(t) \qquad x = -a/2 \tag{3b}$$

$$(\Phi)(x,y,z,t) = V_{y+}(t) \qquad y = +a/2 \tag{3c}$$

$$(\Phi)(x,y,z,t) = V_{y-}(t) \qquad y = -a/2 \tag{3e}$$

$$(\Phi)(x,y,z,t) = V_{z+}(t) \qquad z = +a/2 \tag{3f}$$

$$(\Phi)(x,y,z,t) = V_{z-}(t) \qquad z = -a/2 \tag{3g}$$

in which a is the trap edge dimension, $V_{pq}(t)$ is the voltage applied to the trap electrode, pq, in which $p = x$, y, and z, and q = + or −. For example, $pq = z+$ denotes the trapping electrode at $z = +a/2$. In most cases, the potential due to space charge may be neglected. The potential at time t inside the trap may be obtained by solving Laplace's equation subject to the above boundary conditions:

$$\nabla^2\Phi(x,y,z,t) = \left(\frac{\partial^2}{\partial x^2} + \frac{\partial^2}{\partial y^2} + \frac{\partial^2}{\partial z^2}\right)\Phi(x,y,z,t) = 0 \tag{4}$$

all x, y, and $z > -a/2$ and $< a/2$

Because of the symmetry of the cubic trap, it is not necessary to solve the equation at each time directly. Instead, we need only solve the equation with the following boundary condition, namely, the "base" potential for a constant voltage applied to just one of the six plates of a cubic trap [9].

$$\Phi_{\text{base}}(x,y,z) = 1 \quad x = -a/2$$

$$\Phi_{\text{base}}(x,y,z) = 0 \quad x = a/2,\ y = \pm a/2, \text{ or } z = \pm a/2 \tag{5}$$

The potential for the general boundary condition (Eqs. (1)) may then be expressed as a superimposition of six such "base" potentials, $\Phi_{\text{base}}(x,y,z)$, one for each plate of

the cubic trap.

$$\Phi(x,y,z,t) = V_{x+}(t)\Phi_{\text{base}}(x,y,z) + V_{x-}(t)\Phi_{\text{base}}(-x,y,z) + V_{y+}(t)\Phi_{\text{base}}(y,x,z) + V_{y-}(t)\Phi_{\text{base}}(-y,x,z) + V_{z+}(t)\Phi_{\text{base}}(z,y,x) + V_{z-}(t)\Phi_{\text{base}}(-z,y,x) \quad (6)$$

As it happens, the "base potential" problem can be solved analytically by separation of variables and Fourier expansion [21] to yield

$$\Phi_{\text{base}}(x,y,z) = \frac{16}{\pi^2}\sum_{n=0}^{\infty}\sum_{m=0}^{\infty}\frac{\cos\left[\frac{\pi(2n+1)z}{a}\right]\cos\left[\frac{\pi(2m+1)y}{a}\right]\sinh\left[\frac{\pi(x-a/2)\sqrt{(2n+1)^2+(2m+1)^2}}{a}\right]}{(2n+1)(2m+1)\sinh\left[\pi\sqrt{(2n+1)^2+(2m+1)^2}\right]} \quad (7)$$

Usually, we are interested in ion motion only near the center of the trap. In that limit, the above potential expression may be expanded in a Taylor series about the center of the trap, to yield the following expression accurate to second order in the coordinates.

$$\Phi_{\text{base}}(x,y,z) \approx \frac{\gamma}{2} + \frac{\beta}{2a}x + \frac{\alpha}{4a^2}(2x^2 - (z^2+y^2)) \quad (8)$$

in which a is the trap edge dimension, and γ, β, and α are trap geometry factors: γ = 1/3, β = 0.72167, and α = 2.77373 for a cubic trap [19].

Typically, the trapping potential inside the trap is formed by application of a static trapping voltage, V_{trap}, to each of a pair of opposed "end cap" electrodes. The boundary condition then becomes

$$\Phi_{\text{trap}} = \begin{cases} V_{\text{trap}} & z = +\frac{a}{2} \text{ and } -\frac{a}{2} \\ 0 & \text{otherwise} \end{cases} \quad (9)$$

The trapping potential may therefore be expressed in the well-known form

$$\Phi_{\text{trap}} = V_{\text{trap}}(\Phi)_{\text{base}}(z,y,x) + V_{\text{trap}}\Phi_{\text{base}}(-z,y,x) = Vtrap\left[\gamma - \frac{\alpha}{2a^2}(x^2+y^2-2z^2)\right] \quad (10)$$

For azimuthal dipolar exaltation, Laplace's equation must be solved subject to the boundary conditions

$$\Phi_x = \begin{cases} V_x(t) & x = +\frac{a}{2} \\ -V_x(t) & x = -\frac{a}{2} \end{cases} \quad (11)$$

in which $V_x(t)$ is the excitation voltage applied to one x-electrode, and $-V_x(t)$ is the excitation voltage applied to the opposed x-electrode. It is convenient to analyze Φ_x as the superposition of two potentials,

$$\Phi_x(t) = V_x(t)\Phi_{\text{base}}(x,y,z) - V_x(t)\Phi_{\text{base}}(-x,y,z) = V_x(t)\frac{\beta}{\alpha}x \quad (12)$$

It is clear that the electrostatic trapping potential is approximately axial quadrupolar (Eq. (10)), whereas the azimuthal excitation potential

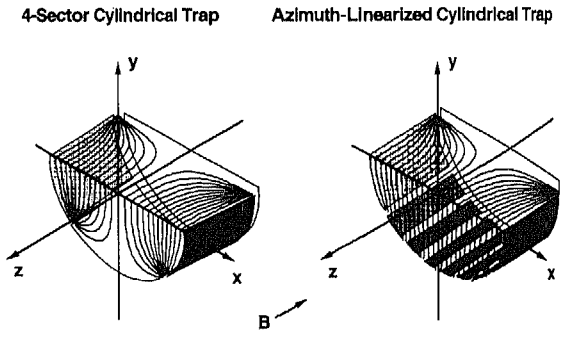

Fig. 3. Comparison of dipolar excitation (or detection) electric isopotentials for a 4-sector cylindrical Penning trap (left) and segmented cylindrical Penning trap (right). One grounded end-cap electrode is shown at the rear of each diagram. By segmenting the excitation (detection) electrodes along the magnetic field direction and applying appropriate potentials to each segment, one can achieve spatially highly uniform excitation (detection) fields (compare isopotentials at the front slice of each diagram).

is approximately dipolar (Eq. (12)). A near-perfectly spatially uniform excitation field (or nearly linear dipolar excitation potential) may be achieved in a "linearized" or "shimmed" trap in which two or more electrodes of a cubic trap are segmented, with different potentials applied to various segments so as to achieve the desired potential inside the trap. For example, Fig. 3 shows a cylindrical trap whose excitation and detection electrodes are segmented, with appropriate voltages applied to the segments so as to generate spatially near-uniform excitation/detection fields.

3.2. Ion motion in the presence of azimuthal dipolar excitation.

The classical motion of an ion in a magnetic field, $\boldsymbol{B}$, and electric field, $\boldsymbol{E}$, is described by the Lorentz equation

$$m\dot{\boldsymbol{v}} = q(\boldsymbol{E} + \boldsymbol{v} \times \boldsymbol{B}) \tag{13}$$

in which m and q are the ion mass and charge, and $\boldsymbol{v}$ ($= \dot{x}\boldsymbol{i} + \dot{y}\boldsymbol{j} + \dot{z}\boldsymbol{k}$) is its velocity. In FT-ICR experiments, $\boldsymbol{B}$ is constant in magnitude and its direction defines the (negative) z-axis: $\boldsymbol{B} = -B\boldsymbol{k}$. ($\boldsymbol{B}$ is taken to point in the negative z-direction, so that the cyclotron orbital angular velocity of a positive ion is positive valued.)

The electric field is the superposition of the (static) trapping and (oscillating) azimuthal dipolar excitation fields. Combining Eqs. (3) and (13) yields

$$\begin{aligned}\boldsymbol{E} &= -\nabla\left[\Phi_{\text{trap}} + \Phi_x\right] \\ &= -\nabla\left[V_{\text{trap}}\left[\gamma - \frac{\alpha}{2a^2}(x^2 + y^2 - 2z^2)\right] + \frac{\beta V_x(t)}{a}x\right] \\ &= \frac{m}{2q}\omega_z^2[x\boldsymbol{i} + y\boldsymbol{j}] - \frac{m}{q}\omega_z^2 z\boldsymbol{k} - \frac{\beta V_x(t)}{a}\boldsymbol{i}\end{aligned} \tag{14}$$

in which

$$\omega_z = \sqrt{\frac{2\alpha q V_{\text{trap}}}{ma^2}} \tag{15}$$

is the frequency of z- or axial oscillation between the two end cap electrodes. In the absence of collisional damping, substitution of Eq. (14) into Eq. (13) leads to independent equations for axial and azimuthal motion

$$\ddot{z} + \omega_z^2 z = 0 \tag{16}$$

$$\ddot{\boldsymbol{r}} - \omega_c \boldsymbol{k} \times \dot{\boldsymbol{r}} - \frac{1}{2}\omega_z^2 \boldsymbol{r} - \phi_x(t)\boldsymbol{i} = 0 \tag{17a}$$

in which

$$\phi_x(t) = \frac{q\beta V_x(t)}{ma} \tag{17b}$$

and

$$\boldsymbol{r} = x\boldsymbol{i} + y\boldsymbol{j} \tag{17c}$$

is the azimuthal (radial) position vector, and

$$\omega_c = \frac{qB}{m}$$

is the unperturbed cyclotron frequency in the absence of any electric field. It is algebraically more compact to express the azimuthal equation (Eqs. (17)) in complex coordinates (x,iy)

$$\ddot{\rho} - \mathrm{i}\omega_c\dot{\rho} - \frac{1}{2}\omega_z^2\rho - \phi_x(t) = 0 \tag{18}$$

in which

$$\rho = x + \mathrm{i}y \tag{19}$$

3.3. V-vector representation of equations of ion cyclotron and magnetron motion

Brown and Gabrielse [12] showed that the azimuthal equation of motion, Eq. (18), can be further simplified by introduction of so-called "V-vectors". The V-vector method is not the only way to solve the equations of ion motion. For example, Mitchell has developed four different alternative transformations [22]. Kretzschmar introduced a related action-angle transformation [23]. Mitchell has derived an equivalent form of the action-angle transformation and applied it to several problems. The advantage of the V-vector method, like normal-mode analysis of vibrational

spectra, is that it conveniently separates the independent ion motional "modes" (cyclotron rotation, magnetron rotation, axial oscillation) and is algebraically compact. For convenience, we define the V-vectors, V^+ and V^- in complex coordinates

$$V^+ \equiv V_x^+ + iV_y^+ = \dot{\rho} - i\omega_- \rho \tag{20a}$$

$$V^- \equiv V_x^- + iV_y^- = \dot{\rho} - i\omega_+ \rho \tag{20b}$$

in which

$$\omega_\pm \equiv \frac{\omega_c}{2} \pm \sqrt{\frac{\omega_c^2}{4} - \frac{\omega_z^2}{2}} \tag{1a,b}$$

and $\omega_c = qB/m$ is the unperturbed cyclotron frequency, ω_+ is the reduced cyclotron frequency, and ω_- is the magnetron frequency. V^+ and V^- represent the cyclotron and magnetron velocities, including both the orbital motion in the absence of power absorption and the time rate of change of cyclotron and magnetron radius due to power absorption. V^+ and V^- may also be thought of as coordinates for cyclotron and magnetron motions treated as independent "normal modes". The position vector, ρ, and its derivative ($\dot{\rho}$) may be recovered as functions of V^+ and V^-

$$\rho = -\frac{i(V^+ - V^-)}{\omega_+ - \omega_-} \tag{21a}$$

and

$$\dot{\rho} = \frac{\omega_+ V^+ - \omega_- V^-}{\omega_+ - \omega_-}$$

The azimuthal equations of motion then become

$$\frac{dV_x^\pm}{dt} + \omega_\pm V_y^\pm - \phi_x(t) = 0 \tag{22a}$$

$$\frac{dV_y^\pm}{dt} - \omega_\pm V_x^\pm = 0 \tag{22b}$$

Finally, by representing the x- and y-components of the cyclotron and magnetron velocities as real and imaginary parts of mathematically complex velocities, V^+ and V^-,

$$V^+ = V_x^+ + iV_y^+ \tag{23a}$$

$$V^- = V_x^- + iV_y^- \tag{23b}$$

we may combine Eqs. (22) to obtain

$$\frac{dV^+}{dt} - i\omega_+ V^+ - \phi_x(t) = 0 \tag{24a}$$

$$\frac{dV^-}{dt} - i\omega_- V^- - \phi_x(t) = 0 \tag{24b}$$

The advantage of the V-vector representation now becomes evident, because the cyclotron and magnetron motions are completely separated, even during dipolar excitation. In the absence of excitation, $\phi_x(t) = 0$, and both the cyclotron and magnetron motions may be considered as circular harmonic oscillators with frequencies, ω_+ and ω_-. In the absence of excitation, the azimuthal position, ρ, may be expressed as a linear combination of the two circular motions

$$\rho \equiv x + iy = \rho_+(t)e^{-i\omega_+ t} + \rho_-(t)e^{-i\omega_- t} \tag{25}$$

in which ρ_+ and ρ_- are complex cyclotron and magnetron positions whose magnitudes represent cyclotron and magnetron radii and whose phases are the initial phases of the two motions. The relation between the cyclotron and magnetron positions and the V-vectors is given by

$$\rho_+(t) = -\frac{iV^+ e^{i\omega_+ t}}{\omega_+ - \omega_-} \tag{26a}$$

$$\rho_-(t) = \frac{iV^- e^{i\omega_- t}}{\omega_+ - \omega_-} \tag{26b}$$

3.4. Secular ion motions in an r.f.-only quadrupole ion trap

An r.f. quadrupole ion trap consists of one ring electrode and two end-cap electrodes. If a fast oscillating electrical quadrupolar potential

$$\phi_0(t) = V_{rf} \cos(\Omega t) \tag{27}$$

is applied to the ring electrode and the end-cap electrode potentials are at ground, the instantaneous potential at radius, $r = \sqrt{x^2 + y^2}$, and axial displacement, z, in the trap is

$$\phi(r,z) = \frac{\phi_0}{2r_0^2}(r^2 - 2z^2) + \frac{\phi_0}{2} \tag{28}$$

in which r_0 is the characteristic radius of the trap (i.e., the smallest distance from the center of the trap to the ring electrode. The smallest distance from the center to the end-cap electrodes is z_0, and $r_0^2 = 2z_0^2$. Ion motion in such a potential may be described by three independent "Mathieu" equations expressed in Cartesian coordinates [24]:

$$\frac{d^2u}{d\xi^2} - 2q_u \cos(2\xi u) = 0 \qquad \xi = \frac{\Omega t}{2} \tag{29a}$$

$$q_u = \frac{4qV_{rf}}{mr_0^2\Omega^2} \qquad u = z \tag{29b}$$

$$q_u = \frac{2qV_{rf}}{mr_0^2\Omega^2} \qquad u = x,\ y \tag{29c}$$

Dehmelt's pseudopotential approach for quadrupole ion traps separates ion motion into a fast oscillating ion motion (at frequency, Ω) in response to the r.f. drive, and a much slower "secular" motion as if ions are moving in an electrostatic "pseudo"-potential [25]. A more general pseudopotential approach has been developed by Gerlich [26]. In the pseudopotential approximation, when q_z is small, e.g. $q_z <$ 0.4, Eq. (29) describing ion axial motion may be treated as a harmonic oscillator

$$\frac{d^2z}{dt^2} + \omega_z^2 z = 0 \tag{30a}$$

$$\omega_z = \frac{q_z\Omega}{2\sqrt{2}} = \frac{\sqrt{2}qV_{rf}}{mr_0^2\Omega} \tag{30b}$$

3.5. Ion motion in response to axial excitation in a quadrupole ion trap

If an axial excitation voltage signal $V_z(t)$ is applied differentially between the end-cap electrodes, it generates a dipolar spatially nearly uniform excitation field inside the trap. The new equation of ion motion may be written as [27]

$$\ddot{z} + \omega_z^2 z = \eta V_z(t) \tag{31a}$$

in which

$$\eta = c_1 q / 2z_0 m \tag{31b}$$

in which $2z_0$ is the distance between the end-cap electrodes and c_1 is a geometric factor for the hyperbolic trap normally used in r.f. ion traps and Penning traps. Gabrielse has computed the value of c_1 to be approximately 0.8 [28]. Finally, we have here discussed the r.f.-only quadrupole ion trap; inclusion of a d.c. component to the quadrupolar potential will change the mass-dependence of the secular frequency, but will not otherwise affect the treatment which follows.

4. Linear response theory applied to ICR spectroscopy

The relation between the input and output of a system defines an engineering specialty called response theory. In spectroscopy, for example, response theory relates power absorption to incident radiation intensity. Although the output of any physical system (say, translational or internal motional amplitude of a molecule or ion) is a non-linear function of the input (e.g., a.c. electric or magnetic field amplitude), the response of any system becomes approximately linear in the limit that the response amplitude is sufficiently small. For example, an electron is bound to a positively charged atomic nucleus by a Coulomb potential; however, if the electron displacement is small, we can treat the force as linear (i.e., a harmonic oscillator) [29]. The generality of linear response theory is that we don't need to know the details of the mechanism involved; any linear system must respond in the same way.

The well-developed theory of linear response traditionally deals with the "forward" process of determining (say) the time-domain response to a

given time-domain driving force (excitation) waveform. However, if the system is linear, then we can propose a desired response, and work backward to determine the excitation waveform that would generate that response. The simplest way to approach the problem is to think of the frequency-domain spectrum (obtained by Fourier transform) of the time-domain excitation waveform. Rather than calculating the excitation spectra of different source time-domain waveforms, we can instead specify a desired frequency-domain excitation spectrum, and then (because Fourier transformation is a linear operation) perform an inverse Fourier transform to generate the corresponding time-domain excitation waveform to produce that spectrum. In the next two sections, we shall explore both the "forward" and "inverse" approaches. In this section, we first show that ions in a Penning trap do indeed exhibit a linear relation between ion motional amplitude (response) to azimuthal dipolar electric excitation. Once it is established that ICR excitation and detection are linearly related, then we can immediately apply linear response theory without further attention to the details of ion motion.

A deterministic physical system is completely described by its equations of motion. Rigorous treatment of linear response of ion cyclotron motion in the absence of an applied electrostatic "trapping" potential was first provided by Guan [30] and extended by Grosshans and Marshall to include the trapping potential [13]. Similarly, we have previously examined the relation between axial a.c. electric field excitation amplitude and ion axial oscillation amplitude in a quadrupole (Paul) ion trap [27]; the theoretical treatment there is quite similar to that for ICR.

Starting from the equations of ion (cyclotron and/or magnetron) motions in the presence of azimuthal dipolar electric excitation, we may now analyze the ion trajectory in response to that excitation. Eq. (24) is a linear differential equation and we may multiply each term by $e^{-i\omega_+ t}$ to yield a more compact equation.

$$\frac{d}{dt}\left[V^+(t)e^{-i\omega_+ t}\right] = \phi_x(t)e^{-i\omega_+ t} \tag{32a}$$

Similarly, we may simplify the magnetron motion (Eq. (24)) by multiplying each term by $e^{-i\omega_+ t}$ to yield

$$\frac{d}{dt}\left[V^-(t)e^{-i\omega_- t}\right] = \phi_x(t)e^{-i\omega_- t} \tag{32b}$$

To find out the final location (at time, t_2) of an ion subjected to excitation during the interval, $t_1 \leq t \leq t_2$, we integrate Eqs. (32) with respect to time over that interval:

$$V^{\pm}(\omega_\pm,\ t=t_2)e^{-iw_\pm t_2} - V^{\pm}(\omega_\pm,\ t=t_1)e^{-i\omega_\pm t_1} = \int_{t_1}^{t_2} \phi_x(\tau)e^{-i\omega_\pm \tau}\, d\tau \tag{33a}$$

in which

$$\begin{cases} \phi_x(t) = \dfrac{q\beta V_x(t)}{ma} & t_1 \leq t \leq t_2 \\ \phi_x(t) = 0 & \text{otherwise} \end{cases} \tag{33b}$$

Now we can use Eqs. (33) to calculate ion trajectories during a cyclotron excitation. For simplicity, let the initial ion cyclotron radius be zero at the onset of excitation ($V^+(\omega_+, t) = 0$ at $t = t_1$)

$$V\pm(\omega_\pm,\ t) = e^{i\omega_\pm t}\int_0^t \phi_x(\tau)e^{-i\omega_\pm \tau}\, d\tau \tag{34}$$

From Eqs. (21), we can then obtain $\rho(t)$ from V^+ and V^- to yield

$$\rho(t) = -\frac{i(V^+ - V^-)}{\omega_+ - \omega_-} = -\frac{i}{\omega_+ - \omega_-} \times \left(e^{i\omega_+ t}\int_0^t \phi_x(\tau)e^{-i\omega_+ \tau} - e^{i\omega_- \tau}\int_0^t \phi_x(\tau)e^{-i\omega_- \tau}\, d\tau\right) \tag{35}$$

From Eq. (35), we may calculate the ion trajectory for any time-domain excitation potential, $\phi_x(t)$. However, we shall next show that the system is linear, so that we can predict the post-excitation cyclotron radius without solving for the ion trajectory directly.

FT-ICR MS experiments are carried out in a pulsed mode: i.e., excitation is applied for a finite duration and then removed during detection. For an excitation pulse whose amplitude is non-zero only during the time period, $t_1 \leq t \leq t_2$, the integration limits in Eq. (35) may be extended to $\pm \infty$. The initial state of cyclotron motion, $V^+(\omega_+, t=t_1)$, and the final state, $V^+(\omega_+, t = t_2)$, are then related by a Fourier transform of the excitation voltage (see Eqs. (33)). Since a Fourier transform is linear, the ICR excitation/response relation is also linear. We have thus derived a general relation between the excitation voltage spectrum and the ion cyclotron motional amplitude.

$$V \pm(\omega_\pm, t_2)e^{-i\omega_+ t_2} - V^+(\omega+, t_1)e^{-i\omega_+ t_1} = \eta' F(\omega_+) \quad (36)$$

in which

$$F(\omega_+) = \int_{-\infty}^{\infty} \phi_x(\tau)e^{-i\omega_+\tau}\, d\tau$$

is the Fourier transform of the time-domain excitation waveform,

$$\eta' = \frac{q\beta}{ma} \quad (37)$$

is a proportionality constant, and

$$F(\omega_+) = \int_{-\infty}^{\infty} V_x(\tau)e^{-i\omega_+\tau}\, d\tau = M(\omega_+)e^{i\Phi(\omega_+)} \quad (38)$$

is the excitation voltage complex spectrum whose magnitude spectrum is $M(\omega)$ and whose phase spectrum is $\Phi(\omega)$. Eq. (36) is the most general relation between an excitation waveform and ion motion, and predicts the ion response to any excitation waveform. For simplicity, we limit ourselves a single excitation "event" per experiment. We further suppose that the initial cyclotron speed is zero, $V^+(\omega, t_1) = 0$, and that the excitation terminates at $t_2 = 0$, which also marks the onset of detection (it is convenient to define the time scale to start detection at time zero). Eq. (36) becomes

$$V^+(\omega_+, 0) = \eta' F(\omega_+) \quad (39)$$

According to Eq. (39), the post-excitation cyclotron radius, ρ_+, is linearly proportional to the excitation voltage spectrum at the reduced cyclotron frequency, ω_+.

$$\rho_+(\omega_+) = -\frac{i\eta'}{\omega_+ - \omega_-}F(\omega_+) \quad (40a)$$

Similarly the magnetron radius is also linearly proportional to the excitation spectrum at the magnetron frequency, ω_-.

$$\rho_-(\omega_-) = \frac{i\eta'}{\omega_+ - \omega_-}F(\omega_-) \quad (40b)$$

Note that the expressions for magnetron and cyclotron motion differ in phase by 180° (i.e., a minus sign).

Eq. (40) indicates that one can obtain the post-excitation cyclotron radius and phase at any given cyclotron frequency by computation of the excitation voltage spectrum at that frequency, as we shall illustrate by several examples in the next section. Conversely, the same equation allows us to synthesize an excitation waveform to produce any desired post-excitation radius and phase. In single-pulse experiments, the post-excitation cyclotron motion phase is usually not extracted, and only the magnitude spectrum, $M(\omega_+)$, need be considered. From Eq. (40)

$$M(\omega_+) = \frac{\omega_+ - \omega_-}{\eta'}|\rho_+(\omega_+)| = \frac{ma(\omega_+ - \omega_-)}{q\beta}|\rho_+(\omega_+)| \quad (41)$$

The excitation voltage magnitude spectrum is therefore proportional to the specified cyclotron radius, $|\rho_+(\omega_+)|$. Typically, the cyclotron frequency is much greater than magnetron frequency, $\omega_+ - \omega_- \approx \omega_+ \approx \omega_c$, and the above equation simplifies to

$$M(\omega_+) \approx \frac{aB}{\beta}|\rho_+(\omega_+)| \quad (42)$$

5. Frequency spectra of some FT-ICR time-domain excitation waveforms

As mentioned in the previous section, linear response theory makes it possible to predict the ion response to a time-domain excitation waveform by Fourier transformation without having to solve the ion equation of motion directly. In this section, we examine the most commonly used FT-ICR excitation waveforms (other than SWIFT waveforms). Single-frequency excitation, commonly used in NMR spectroscopy [1] was used in the first FT-ICR experiment by Comisarow and Marshall [31]. They later introduced frequency-sweep excitation to overcome the bandwidth limit of the single-frequency excitation [32,33]. Frequency-sweep excitation remains the most commonly used excitation method for FT-ICR MS. Impulse excitation (i.e., zero-frequency burst excitation) was used by McIver et al. in 1989 [34]. We next review these FT-ICR excitation methods in a common theoretical format.

A typical FT-ICR excitation waveform may be expressed in the form

$$V_x(t) = \begin{cases} V_0 \cos(\phi(t)) & -T \le t \le 0 \\ 0 & \text{otherwise} \end{cases} \quad (43)$$

In which $V_x(t)$ is the voltage waveform in Eq. (11). T is the duration of the waveform which is chosen to start at $t = -T$ and end at $t = 0$ (notation chosen for convenience in analyzing the response starting at $t = 0$). The phase, $\phi(t)$, of the time-domain waveform may be expressed as a second-order polynomial in t

$$\phi(t) = \gamma' + \beta' t + \alpha' t^2 \quad (44)$$

in which α', β', and γ' are constants. γ' is a phase factor which does not have physical significance and can be neglected (or chosen to be zero) in the following discussion. The excitation waveform, $V_x(t)$, has a rectangular "top-hat" profile whose time-domain amplitude is V_0 for the duration of the waveform, $-T \le t, 0$. Different time-domain waveforms can be classified according to the presence or absence of α' and/or β' coefficients in the phase function of Eq. (44).

5.1. Impulse excitation (β' = O and α' = O)

The simplest time-domain voltage excitation profile is a d.c. pulse of constant amplitude, applied differentially between the opposed pair of excitation electrodes of a cubic trap:

$$V_x(t) = \begin{cases} V_0 & -T \le t \le 0 \\ 0 & \text{otherwise} \end{cases} \quad (45)$$

Its frequency-domain spectrum is readily obtained by Fourier transformation (see Eq. (34)) [29].

$$F(\omega) = V_0 \int_{-T}^{0} e^{-i\omega_+ \tau}\, d\tau = \frac{2V_0}{\omega} e^{-i\omega_+ T/2} \sin\left(\frac{\omega T}{2}\right) \quad (46)$$

The cyclotron radius, $|\rho_+(\omega_+)|$, and magnetron radius, $|\rho_-(\omega_-)|$ may be calculated from

$$|\rho_+(\omega_+)| = \frac{\eta'}{\omega_+ - \omega_-}|F(\omega_+)| = \frac{2V_0\eta'}{\omega_+(\omega_+ - \omega_-)}$$

$$\left|\sin\left(\frac{\omega_+ T}{2}\right)\right| \approx \frac{V_0 T\beta}{aB}\frac{|\sin(\omega_+ T/2)|}{\omega_+ T/2} \quad (46a)$$

$$|\rho_-(\omega_-)| = \frac{\eta'}{\omega_+ - \omega_-}|F(\omega_-)| = \frac{2V_0\eta'}{\omega_-(\omega_+ - \omega_-)}$$

$$\left|\sin\left(\frac{\omega_- T}{2}\right)\right| \approx \frac{V_0 T\beta}{aB}\frac{|\sin(\omega_- T/2)|}{\omega_- T/2} \quad (46b)$$

It is clear that the frequency-domain spectral response (namely, cyclotron or magnetron radius) following an impulse excitation is a sinc function. Fig. 4 shows magnitude-mode spectra in both frequency and m/z domains. For a sufficiently short time duration, T, impulse excitation can excite ions with near-uniform amplitude over a wide m/z range (corresponding to $\approx 0.1/T$ Hz). However, a severe limitation of the method is that ion magnetron radius is excited to the same

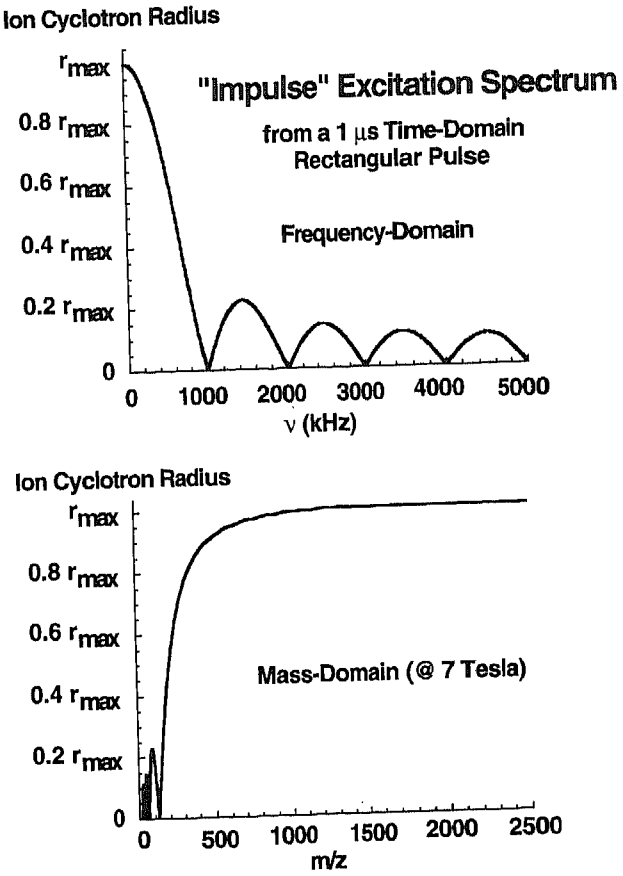

Fig. 4. Ion cyclotron radius (response) following d.c. "impulse" excitation (± 5772 V applied between opposed electrodes in a 2 in cubic ICR ion trap to yield a maximum post-excitation radius, r_{max} = 0.5 in = 1.27 cm at 7 T). Top: Frequency-domain. Bottom: Mass-domain.

extent as its cyclotron radius

$$|\rho_+(\omega_+)| \approx |\rho_-(\omega_-)| \approx \frac{V_0 T \beta}{aB} \qquad (47)$$

Fig. 5 illustrates an ion trajectory following impulse excitation. For ions whose cyclotron frequency, $\nu_+ = \omega_+/2\pi \ll 1/T$ (i.e., ions whose m/z values lie on the flat portion of Fig. 4, bottom), the impulse electric field, $\boldsymbol{E}_{impulse}$, imparts a velocity, $\nu_{impulse} = \boldsymbol{E}_{impulse} \times \boldsymbol{B}/|\boldsymbol{B}|^2$, along a direction perpendicular to the excitation electric field. Immediately after excitation, the ion is moving at $\nu_{impulse}$ as shown in Fig. 5, resulting in a new cyclotron orbit of radius, ρ_+, displaced by ρ_+ (= ρ_-) from the ion's original location.

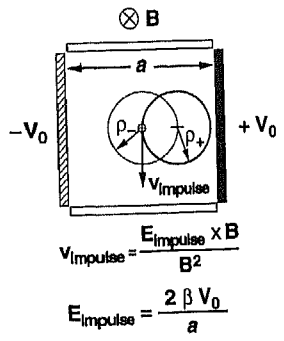

Fig. 5. Ion magnetron and cyclotron radii following impulse excitation. Note that cyclotron and magnetron radii are the same, because the frequency-domain magnitude of the excitation spectrum is the same at both frequencies (see Eq. (47)).

5.2. Single frequency (burst) excitation ($\beta' \neq 0$ and $\alpha' = 0$)

Theoretically, the Fourier transform of a single-frequency pulse is the same as that for a d.c. pulse, except that the spectrum is shifted by the frequency of the pulse. The ion cyclotron radius response to single-frequency excitation at $\beta' = \omega_{excite}$ is given by

$$|\rho_+(\omega_+)| = \frac{\eta'}{\omega_+ - \omega_-}|F(\omega_+ - \omega_{excite})| = \frac{2V_0\eta'}{(\omega_+ - \omega_{excite})(\omega_+ - \omega_-)}\left|\sin\left(\frac{(\omega_+ - \omega_{excite})T}{2}\right)\right| \quad (48)$$

A similar expression describes the magnetron radius response. For "resonant" excitation, namely, $\omega_{excite} = \omega+$), the cyclotron radius is directly proportional to the excitation duration, T.

$$|\rho_+(\omega_+)| = \frac{V_0\eta' T}{\omega_+ - \omega_-} \approx \frac{V_0 T\beta}{aB} \quad (49)$$

The kinetic energy, KE, of the ion undergoing resonant excitation can be expressed as

$$\mathrm{KE} = \frac{1}{2}m|\omega_+\rho_+|^2 \approx \frac{(qV_0T\beta)^2}{2ma^2} \quad (50)$$

Owing to limited bandwidth, lack of selectivity, and need for high excitation voltage, single-frequency excitation is seldom used to excite ions for broadband detection. However, single-frequency excitation is routinely employed for efficient collision-induced dissociation (CID). For example, based on a principle previously demonstrated by Marshall [7], Boering et al. resonantly excited ions of a single mass-to-charge ratio (i.e., single cyclotron frequency) to a large cyclotron radius and then shifted the excitation voltage phase by 180° [8,9]. Prior to the phase shift, ion cyclotron radius increases linearly with time (Eq. (49)). After the excitation phase shift, the ion cyclotron radius decreases with time and eventually returns to zero [7]. The process may be repeated many times to heat ions repeatedly to a specified velocity for very low energy (VLE) collision-induced dissociation. Alternatively, Gauthier, Trutman, and Jacobson achieve CID by applying single-frequency sustained off-resonance irradiation (SORI), at a frequency higher (or lower) than the cyclotron frequency of the ions of interest [10]. Off-resonant excitation accelerates ions sinusoidally out to a larger cyclotron radius and then decelerates them to their starting radius, according to eqn (35) [35] because the phase difference between the excitation field and the cyclotron motion of the ions accumulates continuously, so that the excitation is alternately in- and out-of-phase with the ion cyclotron motion. Finally, Lee et al. have used multiple excitation collisional activation (MECA), in which ions are initially resonantly excited to a large cyclotron radius, followed by removal of excitation to allow the cyclotron motion to damp nearly zero by collisions, followed by additional excitation/relaxation cycles [6].

Fig. 6 illustrates ion trajectories for two activation cycles for each of the three above-mentioned CID techniques based on single-frequency dipolar excitation. It is clear that the three methods share a common strategy, namely periodic modulation of the ion cyclotron radius to a maximum determined by the excitation amplitude. In SORI, the cyclotron radius is returned to zero by the accumulation of phase difference between excitation electric field and cyclotron motion [10]. In VLE, ion cyclotron motion is de-excited by a 180° phase shift of the excitation field [7–9]. In MECA, ion cyclotron radius is reduced by collisions in the absence of excitation. Senko et al. have experimentally compared all three CID methods for dissociation of multiply–charged ions generated from an electrospray ionization source [36].

5.3. Frequency sweep excitation ($\alpha' \neq 0$)

Frequency sweep or "chirp" excitation is the

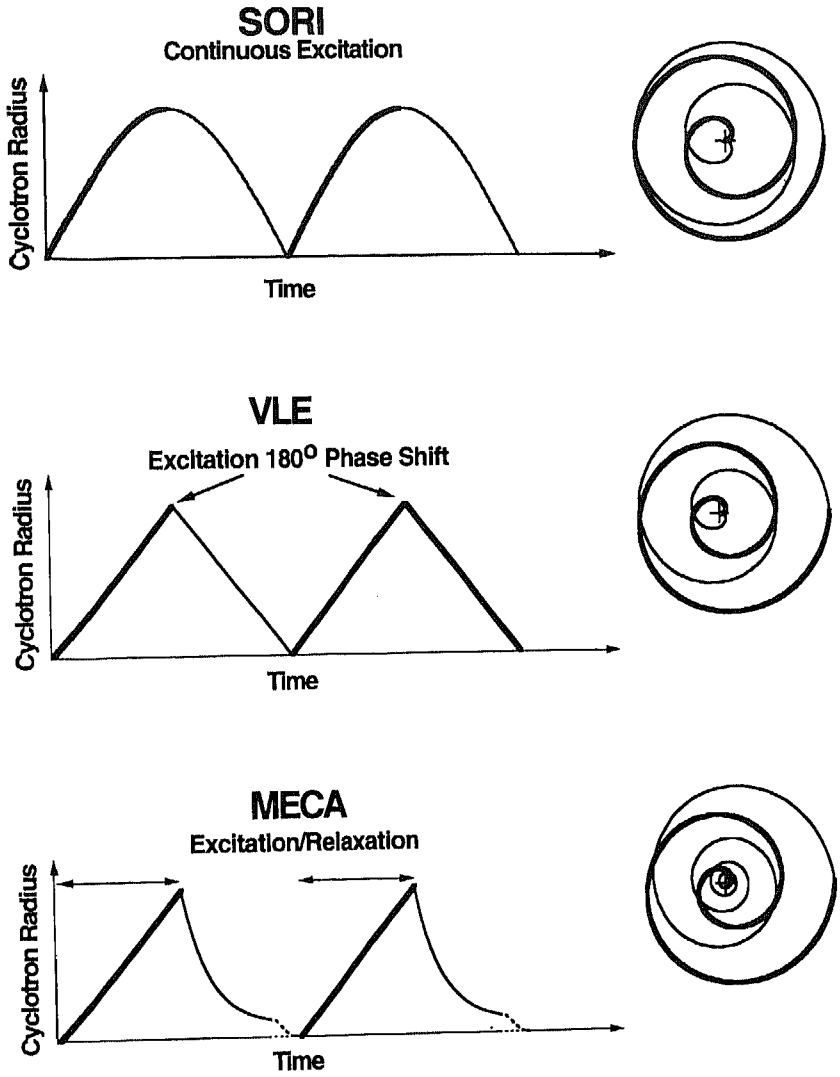

Fig. 6. Time evolution of ion cyclotron radius (left) and ion *xy*-trajectory (right) for each of three ICR techniques for ion multiple activation based on repeated single-frequency dipolar excitation for collision-induced dissociation (CID). In multiple excitation for collisional activation (MECA), ions are resonantly excited and then allowed to relax by collisions. In sustained off-resonance irradiation (SORI), ions are alternately excited and de-excited due to the difference between the excitation frequency and the ion cyclotron frequency. In very low energy (VLE) CID, ions are alternately excited and de-excited by resonant excitation whose phase alternates bimodally between 0° and 180°.

most commonly method of excitation for broadband FT-ICR MS detection. A theoretical analysis of frequency-sweep excitation has been provided by Marshall and Roe [33], and subsequently adapted to excitation of axial secular motion in a quadrupole (Paul) ion trap by Goeringer et al. [37]. Unlike the single-frequency excitation, whose excitation frequency range is determined solely by the duration of the pulse, the bandwidth of a chirp is defined by the two phase parameters (α' and β')

$$\omega_{\text{start}} = \frac{d\phi(t)}{dt}_{t=-T} = \beta' - 2\alpha' T \tag{51}$$

$$\omega_{\text{end}} = \frac{d\phi(t)}{dt}_{t=0} = \beta' \tag{52}$$

which denote the start and end frequencies of the sweep. The frequency sweep rate is the time

derivative of the instantaneous frequency

$$\frac{d\omega(t)}{dt} = \frac{d^2\phi(t)}{dt^2} = 2\alpha' \tag{53}$$

in radians per second, or

$$\frac{1}{2\pi}\frac{d\omega(t)}{dt} = \frac{\alpha'}{\pi} \tag{54}$$

in Hz s^{-1}. The frequency sweep rate is either positive or negative according to the frequency sweep direction. The parameters, α' and β', may be calculated from Eqs. (51) and (52) if the start and end frequencies (ω_{start} and ω_{end}) and the sweep duration, T or the sweep rate, $d\omega(t)/dt$, are given.

From Eq. (42), the ion (cyclotron radius) response to a frequency sweep waveform may be written as

$$|\rho_+(\omega)| \approx \frac{\beta}{aB} M(\omega) \tag{55}$$

in which

$$M(\omega) = \left| \int_{-\infty}^{\infty} V_x(\tau) e^{-i\omega\tau}\, d\tau \right| = \left| V_0 \int_{-T}^{0} \cos(\beta'\tau + \alpha'\tau^2) e^{-i\omega\tau}\, d\tau \right| \tag{56}$$

is the magnitude spectrum of the excitation voltage signal. An integral of the form

$$F(\omega) = \int_{T_1}^{T_2} \exp(\gamma' + \beta'\tau + \alpha'\tau^2)\, d\tau \tag{57}$$

is called a Fresnel integral, whose properties [38] are well-documented in the literature of signal processing. An important feature of chirp excitation is that the excitation magnitude vs. frequency profile does not change dramatically if the product of excitation duration and excitation amplitude is kept constant (see Fig. 7), as a consequence of Parseval's theorem of Fourier analysis.

A linear frequency sweep provides approximately equal excitation power across the frequency range of interest. For resonant excitation of relativistic-speed ions (whose mass increases as their velocity increases, it is necessary to add a cubic term in the excitation phase vs. time function to keep ions on resonance during excitation [39].

6. Stored waveform inverse Fourier transform (SWIFT) excitation

For the FT-ICR excitation methods described

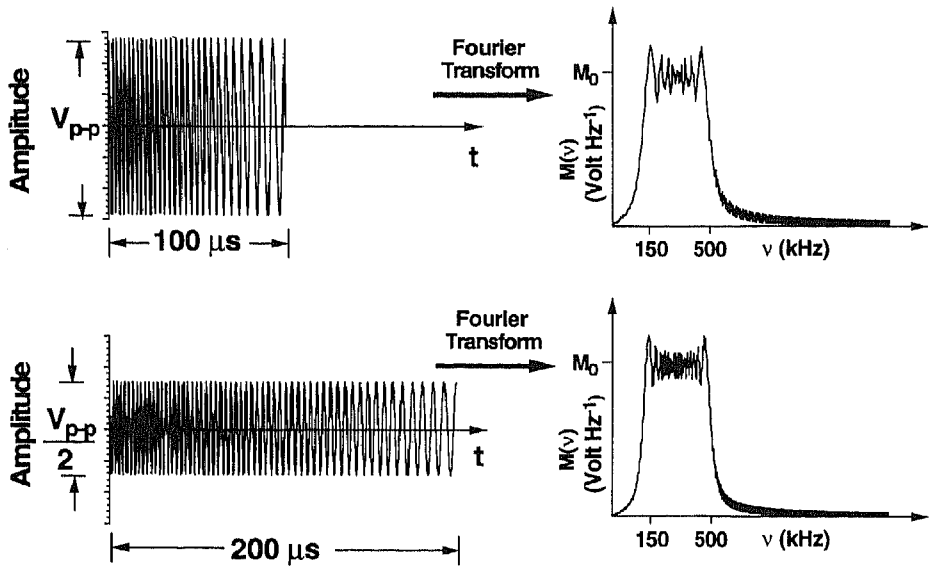

Fig. 7. Time-domain frequency-sweep ("chirp") waveforms (left) and their frequency domain magnitude-mode spectra (right). Note that a shorter and higher-amplitude chirp gives a magnitude spectrum similar to that for a longer and lower-amplitude chirp (see text).

in the previous section, the time-domain waveform is specified first and the corresponding frequency response is analyzed by Fourier transformation of that waveform. A better approach would be to synthesize a time-domain waveform so as to achieve arbitrarily specified initial and final cyclotron states (including radius and phase). Fortunately, by linear response theory, both post-excitation cyclotron radius and phase are linearly related to the magnitude and phase of the excitation waveform. Thus, the desired stored excitation waveform for a specified post-excitation radius magnitude/phase spectrum may be generated by inverse Fourier transform of that spectrum (SWIFT) [5,40,41].

In practice, the choice of a post-excitation magnitude/phase spectrum is limited by experimental and/or theoretical constraints on the time-domain waveform or its corresponding frequency-domain magnitude/phase spectrum. For example, the duration of a time-domain excitation waveform is limited by the experimental event sequence and the maximum discrete data size, and its amplitude is limited by the excitation power amplifier. Dynamic range is limited both by the word length of the stored time-domain waveform and the analog power amplifier. There is a trade-off between mass selectivity and magnitude uniformity across a given m/z range. To simplify the problem, we assume that excitation field in the ion trap is spatially uniform and linearly related to the excitation voltage. These requirements are effectively realized with a linearized ICR trap and an excitation power amplifier with near-zero amplitude and phase distortion over the frequency range of interest. In the ensuing sections, we examine the various constraints in SWIFT waveform design, and list methods and algorithms for optimizing a SWIFT time-domain waveform.

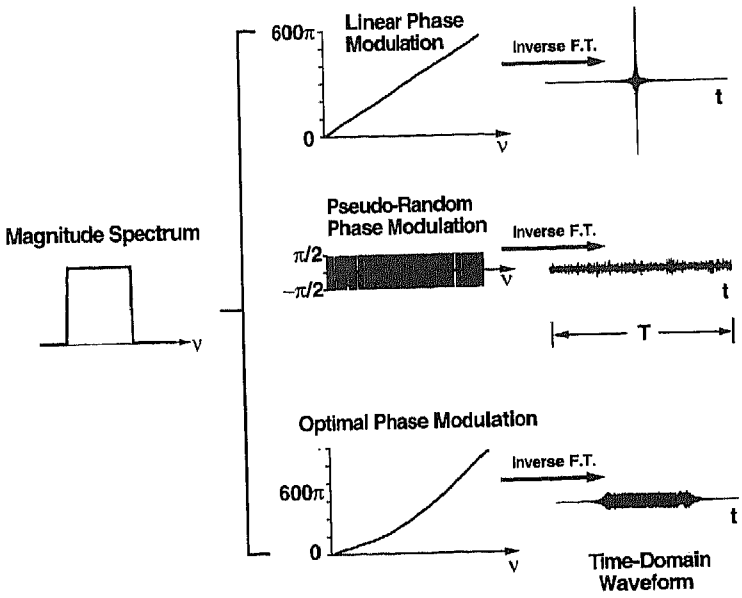

Fig. 8. Three phase vs. frequency functions (middle) and their corresponding SWIFT time-domain waveforms (right) synthesized from each phase function and a rectangular magnitude vs. frequency profile (left). A linear phase spectrum shifts the time-domain power to the center of the SWIFT waveform, with a sharply peaked high-amplitude sinc envelope. A pseudorandom phase spectrum distributes power evenly over the SWIFT excitation period, T. An "optimized" phase spectrum (see text) centers and distributes the time-domain power to reduce the maximum time-domain amplitude while also reducing the time-domain amplitude to near zero at the beginning and end of the SWIFT waveform for reduced distortion (see text).

6.1. SWIFT time-domain waveform amplitude reduction

According to linear response theory, both post-excitation ion cyclotron radius and phase (i.e., the ICR response) are linearly related to the magnitude and phase of excitation voltage spectrum. However, in most applications, the primary goal is a desired post-excitation cyclotron radius vs. cyclotron frequency profile. Because radius and phase are specified independently, we are therefore left to decide on an appropriate cyclotron phase spectrum. The immediate problem is that FT-ICR MS presents a potentially very wide frequency bandwidth: ions of $10 \leq m/z \leq 10\,000$ span a cyclotron frequency range of ≈ 10 kHz to ≈ 6 MHz at 7 T. Thus, if the phase spectrum were chosen to be flat or linear (see Fig. 8, top) with frequency, then excitation of ions to 1 cm of cyclotron radius over a frequency range of 6 MHz would require generation of a time-domain excitation waveform with an r.f. amplitude of over 50 000 V applied across a 2 in (5.08 cm) cubic trap, a voltage amplitude not easily produced experimentally.

In their original paper, Tomlinson and Hill considered the time-domain amplitude issue, and proposed a phase spectrum which alternates randomly between $-\pi/2$ and $+\pi/2$ (Fig. 8, middle) [5]. Their pseudo-phase modulated time-domain waveform maximum amplitude could thereby be reduced by several orders of magnitude compared to that for constant or linear phase vs. frequency. However, the phase discontinuities and truncation of the time-domain waveform can lead to significant spectral distortion.

Modern SWIFT algorithms therefore specify a magnitude spectrum (which may be *discontinuous*, to allow for excitation/ejection of ions of one or more m/z values without affecting ions of other m/z value(s)), but a phase spectrum that is a *continuous* function of frequency. Fig. 8 illustrates three phase modulation methods. Chen et al. first noted that a *nonlinear* continuous phase spectrum can reduce the maximum amplitude of a time-domain SWIFT waveform [42]. In particular, they demonstrated that a quadratic phase vs. frequency spectrum yields a time-domain SWIFT waveform of near-flat amplitude envelope. Guan subsequently developed a more general phase modulation scheme based on the shift theorem of Fourier analysis as follows [43]. A time-domain waveform constructed from magnitude spectrum whose phase varies linearly with frequency can be thought of as a "wave packet", whose energy is concentrated over a time interval centered at a time determined by the slope of the phase spectrum. Therefore, if the frequency-domain magnitude spectrum is divided into two segments [whose power spectra (the power spectrum is the square of the magnitude spectrum) have equal area] and the phase spectrum is linear (but with different slope) in each of the segments, then the time-domain SWIFT waveform will consist of a superposition of two "wave packets" separated in time. If the phase spectral slopes are sufficiently different, then the two "wave packets" will be separated far enough not to overlap, and the maximum time-domain SWIFT amplitude will be reduced by a factor of about two. Following this argument to its extreme, the magnitude spectrum can be further divided into many segments of equal power spectral area, each with a phase spectrum of different (linear) slope. By choosing the slopes of successive phase spectral segments appropriately, we can shift the time location of the successive corresponding wave packets so that they barely overlap, thereby achieving optimal reduction of the time-domain maximum amplitude. For the simplest case of a single-segment flat magnitude spectrum ("top-hat" or "rectangular" spectrum), this approach reduces to the above-mentioned quadratic phase vs. frequency spectrum. An analytical expression for optimal phase modulation has been given by Guan and McIver [44]. A similar phase modulation method in discrete form was developed independently by Goodman and Hanna [45]. A few examples of the effect of the shape of the phase spectrum on

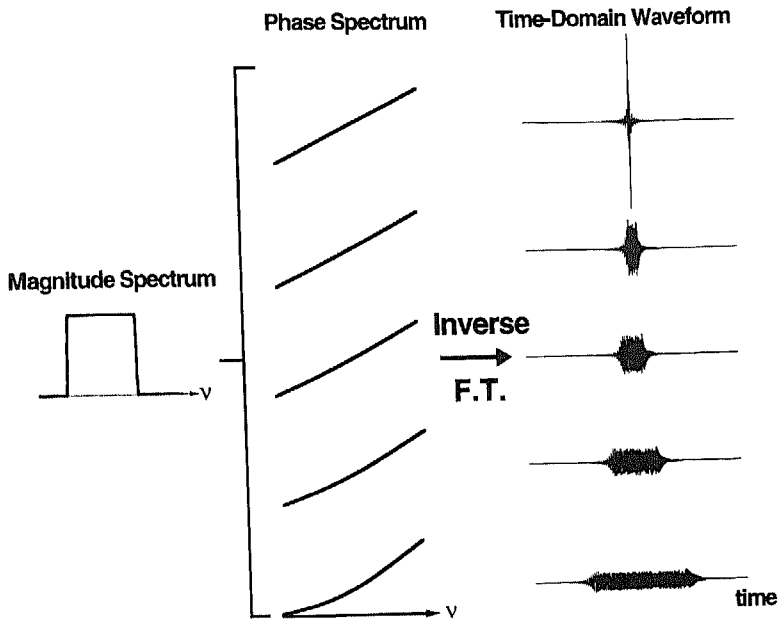

Fig. 9. Effect of addition of a quadratic term of increasing amplitude to a linear phase vs. frequency spectrum on SWIFT waveforms generated as in Fig. 8. Note that increasing the quadratic term spreads out the power (and thus reduces the maximum amplitude) of the SWIFT waveform.

the resultant SWIFT waveform are presented in Fig. 9.

6.2. Excitation smoothness and selectivity

A true time-domain representation of a magnitude vs. frequency profile would require a time-domain waveform of infinite duration. In practice, the finite duration of an actual SWIFT waveform results in two kinds of distortion from the desired magnitude spectrum: magnitude wiggles (particularly near any sharp edges in the magnitude spectrum), and "leakage" of magnitude from spectral segments of high magnitude into spectral segments of low or zero magnitude. Mathematically, an actual SWIFT waveform may be thought of as the product of the "true" (i.e., infinite-duration) waveform by a "top-hat" ("rectangular") weight function. The convolution theorem of Fourier analysis reveals that the spectrum of the product of two time-domain functions is the convolution of their separate spectra. Since the Fourier transform of a "top-hat" function is a sinc function, the effect of such convolution is to introduce wiggles ("Gibb's oscillations") and "leakage" near any sharp edges in the desired magnitude spectrum. We cannot see the "wiggles" simply by taking a forward Fourier transform of a discrete SWIFT waveform, because that would just regenerate the original discrete magnitude spectrum that we started with. However, it is possible to render the "wiggles" visible by "padding" the time-domain SWIFT waveform with an equal number of zeroes (so-called "zero-filling") before performing a forward Fourier transform. With these ideas, we are now ready to examine the "wiggles" and methods for their suppression.

Chen et al. generated a SWIFT waveform by quadratic phase modulation before inverse FT, then reflected the SWIFT waveform about its center (to concentrate signal at the middle of the waveform), and then multiplied the time-domain SWIFT waveform by one quarter-cycle of a sine function at each end of the waveform [42]. Although this method does reduce Gibb's oscillations in the corresponding zero-filled/F.T. magnitude spectrum, the combination

of quadratic phase encodement and apodization produces somewhat different smoothing for different "edges" in the magnitude spectrum. Goodman and Hanna created a SWIFT waveform from a magnitude spectrum and linear phase spectrum (to shift the power to the center of the time-domain waveform), then weighted the time-domain waveform, then Fourier transformed back to the frequency-domain to produce a magnitude-mode spectrum whose phase spectrum was then replaced by a quadratic phase spectrum before a final inverse F.T. to yield an apodized time-domain SWIFT waveform. This more complicated procedure of Goodman and Hanna produces equal smoothing to sharp edges at different frequencies, but (since ICR frequency varies inversely with m/z) smoothing which differs for ions of different m/z [45].

A more general spectral smoothing method, proposed by Guan and McIver [44], applies smoothing to the original magnitude spectrum. Let $M(\omega)$ denote the unsmoothed magnitude spectrum and $\Delta\omega$ denote the width of the smoothing filter, defined according to

$$M_s(\omega) = \frac{1}{\Delta\omega}\int_{\omega-\Delta\omega/2}^{\omega+\Delta\omega/2} M(x)\,dx$$

$$\omega_0 + \Delta\omega/2 < \omega < \omega_1 - \Delta\omega/2 \qquad (58)$$

Notice that if $M(\omega)$ is defined over the range, $\omega_0 \leq \omega \leq \omega_1$, $M_s(\omega)$ can differ from $M(\omega)$ only over the range, $\omega_0+\Delta\omega/2 \leq \omega \leq \omega_1-\Delta\omega/2$. In principle, any smoothing technique can be used. (Goodman and Hanna's IFT-windowing-FFT procedure is an example.) The Guan method is essentially a moving average with a weight factor, and offers several advantages over time-domain apodization-based algorithms. First, the degree of "smoothness" can be varied in the frequency domain by varying the weight factor with frequency. Thus, different magnitude frequency-domain spectral "edges" may be smoothed differently [46], to provide for equal (or different) mass selectivity at different edges. Second, the effect of the smoothing filter may be evaluated analytically in both frequency- and time-domains. Frequency-domain smoothing is the convolution of the magnitude spectrum with a "top-hat" (rectangular) pulse. In the time-domain, the unsmoothed waveform is multiplied by a sinc function which is the Fourier transform of the frequency-domain rectangular weight function. The effect is to decrease the amplitude of the time-domain SWIFT waveform near its initial and final portions. Smoothing width and number of smoothings have different effects on the resulting excitation spectra, as shown in

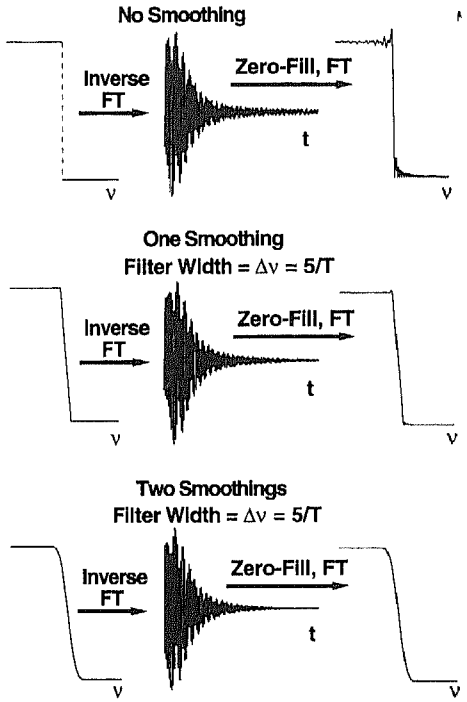

Fig. 10. Effect of magnitude spectral smoothing on the time-domain SWIFT waveform (middle) and its zero-filled Fourier transform "true" magnitude spectrum (right). In these diagrams, only the "edge" segment of the magnitude spectrum and only the "shoulder" of The corresponding time-domain SWIFT waveform are shown. Top: No smoothing. Middle: One smoothing (filter width, $\Delta\nu = \Delta\omega/2\pi = 5/T$, in Eq. (58), with T defined in Fig. 8). Bottom: Two successive smoothings, filter width $5/T$. Note that magnitude spectral smoothing leads to a steeper drop in SWIFT time-domain amplitude near the edges of the time-domain waveform, and thus reduced wiggles (Gibb's oscillations) in the true excitation magnitude spectrum. The smoothing procedure may be repeated many times to achieve any degree of "smoothness", at the expense of reduced selectivity ("sharpness" of edges) in the mass-domain or frequency-domain excitation spectrum.

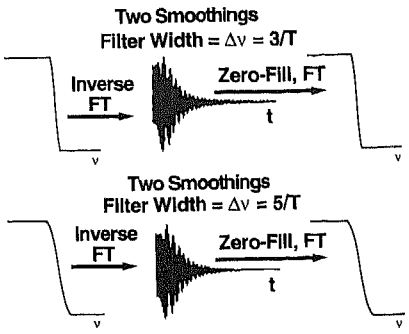

Fig. 11. Effect of filter width in smoothing the magnitude excitation spectrum of a SWIFT time-domain waveform. Presentation is as in Fig. 10. Note that the wider filter width reduces the time-domain SWIFT amplitude at its shoulder, and smooths the resulting magnitude-mode excitation spectrum.

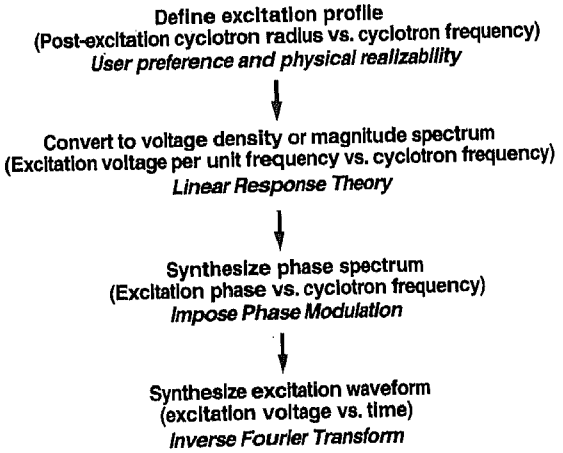

Fig. 12. Algorithm for direct synthesis of a SWIFT waveform (see text).

Figs. 10 and 11. Note that because the smoothing operation is applied only to the frequency-domain magnitude spectrum specified by the user, it is easy to recover the original magnitude spectrum. The inverse operation (or "desmoothing" procedure) may be obtained from the frequency derivative of Eq. (58).

$$M(\omega) = \left(\frac{dM_s(x)}{dx}_{x=\omega-\Delta\omega/2} \right) \Delta\omega + M(\omega - \Delta\omega) \tag{59}$$

Notice that the current value of $M(\omega)$ depends not only on the past value of $dM_s(\omega)/d\omega$ but also on its own past value, $M(\omega-\Delta\omega)$. Both smoothing and desmoothing procedures are readily implemented in any of several computer language codes.

6.3. Complete SWIFT algorithms

Since the effects of both phase modulation and spectral smoothing procedures on a SWIFT time-domain waveform are deterministically predictable, a non-iterative algorithm (Fig. 12) is available. First, the user can construct a desired post-excitation cyclotron radius mass-domain spectrum by combining a series of rectangular magnitude vs. mass segments. After smoothing (in the mass-domain) as described above, the corresponding frequency-domain radius spectrum can be obtained by mass-to-frequency conversion of the abscissa and (by linear response theory) conversion of the ordinate from post-excitation radius to excitation voltage magnitude. The phase spectrum can be constructed by use of Eq. (3) of Ref. [44]. Inverse Fourier transformation of the magnitude and phase spectra then gives the time-domain SWIFT excitation waveform (in the form of voltage vs. time). The actual excitation spectrum can be visualized by zero-filling the SWIFT time-domain waveform and proceeding in reverse of the original waveform synthesis procedures to obtain a mass-domain excitation spectrum. This procedure is illustrated in Fig. 13.

7. Hardware generation of excitation waveforms

In principle, SWIFT excitation incorporates all other excitation waveforms as subsets, because any time-domain waveform may be equally well represented in the frequency-domain for a linear system. For an FT-ICR mass spectrometer operating at 7 T, ions of $10 < m/z < 10\,000$ span cyclotron frequencies from 10 Mz to 10 kHz. Waveforms in this low-frequency AM (amplitude modulation) range may be conveniently

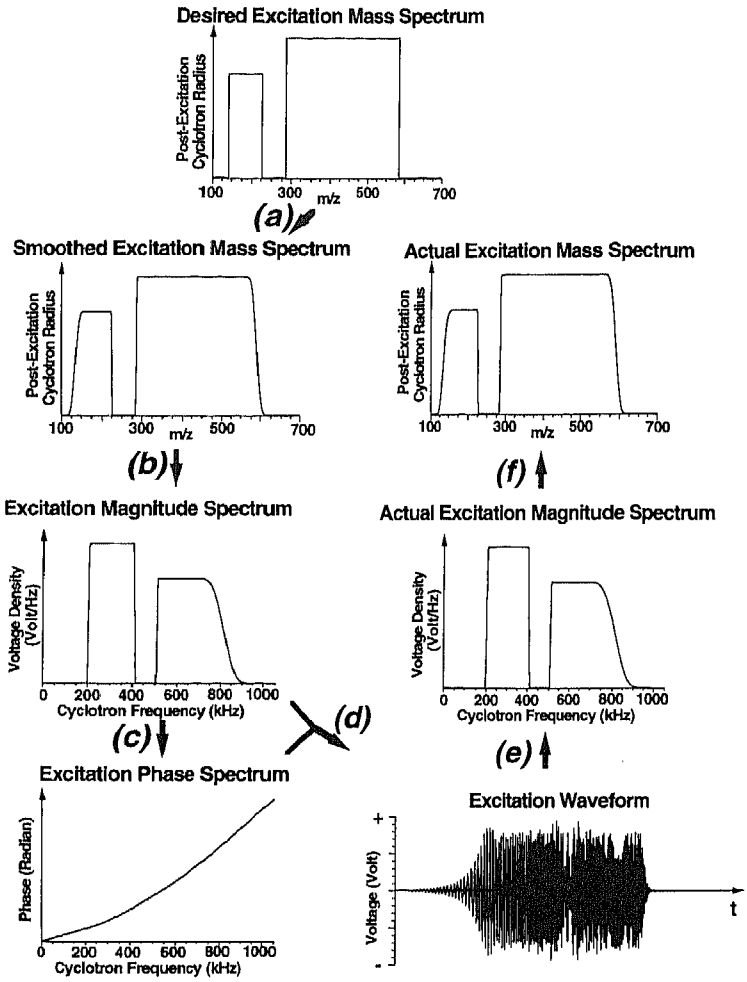

Fig. 13. Step-by-step synthesis of a SWIFT waveform (see text).

generated by TTL circuits, and many commercially available arbitrary waveform generators (AWG) can be used for generation of SWIFT waveforms, subject to appropriate patents. An arbitrary waveform generator normally consists of a static memory bank of 16 kword to 1 Mword, an 8–12 bit digital-to-analog converter, and an address counter which increments the memory locations during excitation. Typical maximum data update rates vary from 1–20 megasamples per second for a commercial AWG module, corresponding to the maximum output frequencies of 0.5–10 MHz. An important aspect of the hardware is the interface between the waveform memory and the computer which controls the experiment. Given that a SWIFT waveform can occupy up to a few megawords of memory, efficient data transfer between the waveform memory and computer system memory is required. The amplitude uniformity of the magnitude excitation spectrum produced by a SWIFT waveform depends directly on the dynamic range of the digital-to-analog converter from which the analog SWIFT voltage is generated [47].

The first SWIFT module was a home-built circuit which was interfaced to a Nicolet 1180 or 1280 computer through an S100 bus [40]. A more detailed description of SWIFT generation

hardware can be found in Ref. [48], in which a 16 kword memory was directly mapped into the computer memory via a PC-compatible ISA (industry standard architecture) bus. Adaptation of a commercial AWG through GPIB (general purpose interface bus) for FT-ICR experiments has also been demonstrated [49,50]. In our own current home-built data system, we employ a VXI arbitrary waveform generator module, whose addresses are generated by a DDS (direct digital synthesis) clock which offers a frequency selectivity of microhertz. DDS is essentially the method that is used for synthesis of frequency-sweep waveforms. Impulse excitation requiring an amplitude of > 1000 V peak-to-peak [34] may be generated by use of high power MOSFET (metal oxide semiconductor field effect transistor) switches.

Analog excitation signals of desired voltage may also be generated by a video power amplifier. In principle, the load impedance of the power amplifier is near-infinite and the amplifier for electron beam deflection in a cathode ray tube (CRT), which can normally deliver several hundred volts output with broad bandwidth and good linearity, would be ideal. However, because the ICR ion trap is typically located ≥ 1 m from the amplifier, the impedance loss due to the transmitter cables can be severe. In order to maintain high linearity over a large bandwidth, a high power (> 50 W) amplifier is usually required. In most applications, two 180° out-of-phase excitation channels are needed (or an r.f. transformer driven by a single channel amplifier).

8. Applications of FT-ICR SWIFT excitation

8.1. Mass-selective ion excitation in ICR

The most basic function of ICR excitation is to increase ion cyclotron radii and produce spatial (and thus temporal) coherence of the cyclotron motion for ion detection. SWIFT excitation can provide uniform-amplitude excitation over a wide frequency range (and thus uniform ion cyclotron radius and uniform ICR signal for equal numbers of ions), and is therefore well-suited for quantitative determination of ion relative abundances. However, for precise measurement of ion numbers, the electric field for both excitation and (by "reciprocity") detection must be spatially uniform anywhere in the trap, and ion initial cyclotron radii should be zero. To a large extent, these requirements are now achievable experimentally. A uniform excitation field can be provided by use of a linearized trap [51–54]. Ion initial cyclotron motion can be cooled by ion–neutral collisions before excitation/ detection events.

For broadband (direct-mode) detection, the highest available frequency (or lowest mass) is limited by hardware, including analog electronic circuitry, analog-to-digital converter, and associated digital electronics such as memory buffers, etc. In heterodyne mode, the location of the detection bandwidth is determined by the reference frequency, whereas the bandwidth during extended data acquisition period is limited by acquisition memory size. Frequency-selective excitation is needed to define the center and width of the frequency band to prevent signals from outside of frequency band from "folding over" into the detection range [29]. Mass-selective SWIFT excitation has proved especially helpful for sorting ion–molecule reactions for metal cluster ions, for which clusters of various size with various numbers of ligands are present [55]. Smalley et al. have used a "comb" SWIFT excitation to select and react individual isotopic species from clusters of several sizes simultaneously [56].

8.2. Mass-selective ion ejection in ICR

One of the unique capabilities of FT-ICR mass spectrometry is its ability to isolate ions over a specified m/z range with high mass selectivity. Ions differing by less than 1 part in 10000 in mass-to-charge ratio may be subjected to

completely different excitation levels in a single event [57]. SWIFT selective ejection can therefore be used to extend dynamic range [58] by several orders of magnitude. The need for removing ions of unwanted m/z will now be discussed briefly.

As the number of ions confined in an ICR trap increases, space charge effects can become severe, with three consequences: shift of detected cyclotron frequency, drift of the cyclotron frequency during detection, and coalescence of closely spaced resonances. In the worst case, the space charge potential along the magnetic field direction can become larger than the electrostatic trapping potential, and ions are no longer trapped. The static frequency shift arises from the trapping potential distortion by space charge. At equilibrium, an ion cloud consisting of ions of a single mass-to-charge ratio behaves as an ellipsoid of constant charge density. The axial potential generated by the space charge is an inverted parabola, and the total electrostatic potential (namely, the sum of the applied electrostatic parabolic axial potential and space charge potentials) retains the same functional form but with a reduced magnitude. The space charge effect on the mass-to-charge ratio measurement can be reduced by adding a space charge term in the mass calibration equation [59]. Frequency drift during ion detection, observed at higher trapping potential and large number of ions, severely degrades mass resolving power. For isolated peaks, frequency drift can be modeled by a simple polynomial, and a digital heterodyne algorithm used to eliminate frequency drift from the final spectrum [60]. Perhaps the most severe effect of space charge is that ICR signals from ions of nearly the same m/z ratio appear as a single coalesced resonance, even though the peak width may be much less than the theoretical peak separation [61]. The peak coalescence effect is particularly troublesome after ions have been axialized prior to high resolution detection [62].

Most FT-ICR mass spectrometers operate at a magnetic field of 3–7 T, with an ICR ion trap (cylindrical or cubic) of $\approx$ 5 cm diameter. The total number of charges in such a trap must be kept below $\sim 10^6$ in order to achieve good mass resolution and mass accuracy. On the other hand, $\approx$ 50 singly charged ions of the same m/z ratio are required to obtain a signal with a signal-to-noise ratio of 2 in a single 1 s acquisition. Thus, high-resolution direct mass analysis of a mixture containing hundreds or thousands of components is difficult, especially for minor components. For such problems, SWIFT mass-selective ejection can improve the situation dramatically. For example, Fig. 14 (top) shows a crude oil distillate broadband mass spectrum produced by low-energy electron impact ionization (to avoid fragmentation of the ions). Obviously, this sample contains species of comparable abundance at every nominal mass from $100 < m/z < 500$ (and in fact several species at each nominal mass, as we shall see). High-resolution detection over such a wide mass range with such a large number of ions was not feasible on that instrument. We therefore tailored SWIFT ejection waveforms to excite ions outside a specified mass-to-charge ratio range to ion cyclotron radii larger than the trap dimension (i.e., ejection from the trap). Note that the isolated ions retain essentially the same abundance profile after isolation, showing that they are unaffected by removal of the unwanted other ions (Fig. 14, second from top). It is even possible to isolate ions of a single common nominal mass by application of a second narrower-band SWIFT ejection (Fig. 14, third from top). A subsequent ultrahigh-resolution heterodyne FT-ICR mass spectrum of those ions (Fig. 14 bottom) yields ion masses accurate to 1 ppm, from which the chemical formulas of Ions of $m/z \leq 400$ may be determined with near certainty. In a series of such experiments, we examined a series of mass spectral segments of $\sim$20 u each, at average mass resolving power of $> 250\,000$ and mass inaccuracy less than 1 ppm. The 20 m/z window could be moved across the full mass spectrum, yielding thousands of chemical formulas from this unusually complex mixture [63].

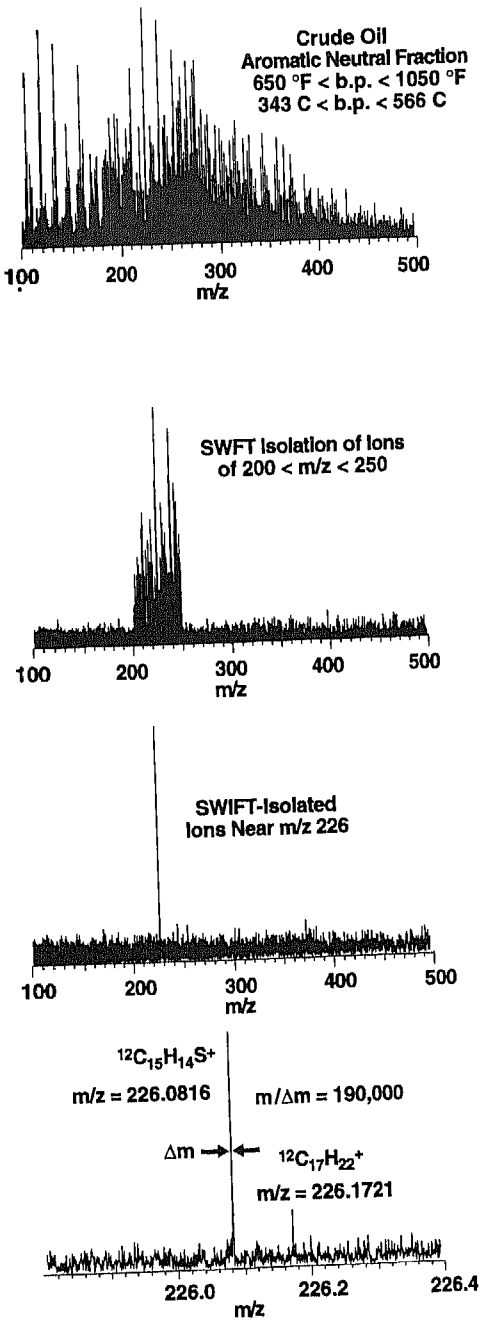

Fig. 14. SWIFT mass-selective ejection for ultrahigh-resolution FT-ICR mass analysis of a complex mixture. Top: Low-energy electron ionization mass spectrum of a crude oil distillate. Second from top: Mass spectrum following broadband "coarse" SWIFT ejection of ions of all but $200 < m/z < 250$ u. Third from top: mass spectrum following narrowband "fine" SWIFT ejection of all of the remaining ions except ions of $m/z \approx 226$. Bottom: ultrahigh-resolution mass spectrum showing baseline resolution of species differing in chemical formula by C_2H_8 vs. S (both approximately 32 u).

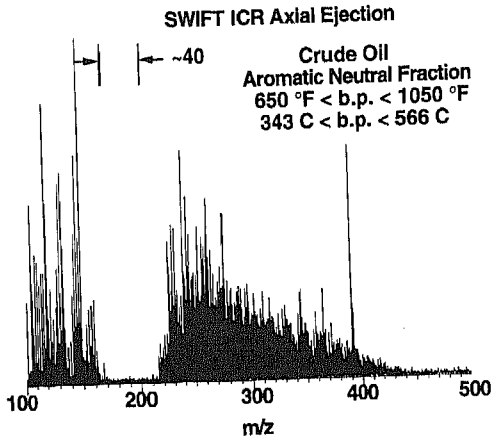

Fig. 15. SWIFT mass-selective ejection by excitation of ion axial motion, for the sample shown in Fig. 14 (top). The duration of the SWIFT time-domain waveform is 20 s, resulting in an m/z ratio selectivity of about 20, which is several orders of magnitude smaller than that for radial ejection by excitation of ion cyclotron motion.

Selective excitation and ejection with ion axial motion are common practice in atomic Penning trap spectroscopy in which cyclotron frequency for a small charged particle, such as an electron or proton, is too high for control and measurement. As seen in Fig. 2, the *axial oscillation* frequency is inversely proportional to the square root of the mass-to-charge ratio. m/z-selectivity based on axial oscillation frequency is thus expected to be poor compared to that for cyclotron motion (whose frequency is inversely proportional to m/z). For such problems, axial ejection offers an effective way to remove electrons or protons from the trap. Fig. 15 shows the effect of a 20 s duration SWIFT waveform applied between the two end caps (additional biased at an electrostatic potential of +2 V) of an ICR (Penning) trap. Although the ejection region was specified to be from $180 < m/z < 200$, ions from $165 < m/z < 215$ were actually found to be ejected. In any case, a potential advantage of axial ejection is that any ions remaining in the trap cannot have been excited to a kinetic energy greater than the trapping potential (i.e., a few volts). Severe heating and collision induced dissociation (always a concern

for radial ejection at kinetic energies of up to 1 keV) are thereby eliminated.

At very high ion density, Coulomb interactions become more important and the equations of ion motion are no longer linear. Cyclotron radius modulation by space charge effects has been studied by several authors [61,64–66]. The assumption of linear response is no longer valid at such high charge density. Similarly, frequency selectivity in Haebel et al.'s high front-end resolution FI-ICR MS/MS experiments may be limited by space charge effects [67,68].

8.3. SWIFT-based two-dimensional FT-ICR mass spectrometry

A particularly nice example of SWIFT-based excitation is the two-dimensional FT-ICR experiment recently demonstrated by Ross et al. [69]. Briefly, the idea (like two-dimensional NOESY FT-NMR) is to excite *all* possible parent ions in a mixture so as to induce them to fragment or react by ion–neutral collisions. The trick is to perform a series of such broad-band excitation experiments, but with different (sinusoidally encoded) excitation magnitude spectra. The required series of SWIFT waveforms can be generated and stored in advance, and the ensuing two-dimensional data array then acquired automatically. Here the use of SWIFT is novel (and essential) in generating data from which *all* parent–product ion–neutral reaction and fragmentation reactions can be identified and quantified in a single automated experiment.

8.4. Mass-selective ion ejection in r.f.-only quadrupole (Paul) ion traps: overmodulation and filtered noise field

Ion motion in a spatially inhomogeneous rapidly oscillating electric field is the basis for many ion transport and storage devices. In an r.f. quadrupole ion trap (QIT), an r.f. voltage is applied to a ring electrode with respect to the two end cap electrodes [24]. Ion motion in such a fast oscillating electrical field may be analyzed into a fast oscillation in response to the r.f. driving field and a much slower "secular" periodic motion. For certain operating conditions and ion m/z range, the amplitude of the fast motion is small and ion motion can be treated as if ions are moving in an electrostatic "pseudo"-potential [25]. In a quadrupole ion trap, the pseudopotential is parabolic in three directions, and ion motion may be treated as harmonic oscillations. Because of the cylindrical symmetry of the trap, there are two different secular or harmonic frequencies for any given operating condition and ion mass-to-charge ratio. The secular frequency is inversely proportional to mass-to-charge ratio of ions (i.e., exactly as for ICR), and the system is sufficiently linear to justify use of linear response theory. (We shall limit our discussion here to the so-called "r.f.-only" quadrupole ion trap; addition of an electrostatic potential of the same symmetry changes the m/z-dependence of the secular frequencies [24], but does not otherwise affect the applicability of SWIFT waveforms.)

In most quadrupole ion trap experiments, ion axial (rather than radial) secular motion is used for mass selection, excitation, and scanning, because it is easier to produce a near-uniform dipolar excitation field along the axial than the radial direction. Ions are typically detected by ejection through a hole in the middle of one of the end cap electrodes into an electron multiplier. Excitation of ion axial secular motion in an r.f.-only quadrupole ion trap may be treated in the same manner as for cyclotron motion discussed above.

As in FT-ICR MS, the volume inside a QIT is limited and space charge effects can be very severe. When a QIT is interfaced to a continuous ion source such as a fast atom bombardment or electrospray ion source, it is very important to eject unwanted matrix or solvent ions from the trap continuously during the ionization period. Mass-selective ion ejection is therefore essential to optimal QIT performance. Theoretical analysis

of ion axial excitation in a QIT is however more difficult than for ICR, because a QIT usually operates at a much higher neutral pressure ($\approx 10^{-3}$ Torr) than for FT-ICR ($\leq 10^{-8}$ Torr), and collisional damping *during* an excitation event cannot be neglected.

Nevertheless, several kinds of time-domain waveforms have been used experimentally to achieve broadband excitation or ejection of ion axial secular motion. Buttrill et al. demonstrated that signal-to-noise ratio is improved by mass-selective ejection for analysis of polychlorinated biphenyls (PCBs) at the femtogram level [70]. Soni and Cooks used a series of repeated SWIFT ejection waveforms to improve signal-to-noise ratio, resolution, and sensitivity of secondary ions generated by Cs^+ ion beam bombardment of a sample dissolved in glycerol [71]. Goeringer et al. adapted Kelley's "filtered noise field" method [72] (see below) for mass-selective ion accumulation [73].

Analysis of some of the waveforms currently used in QIT ion ejection requires us to return to the issue of phase modulation in the generation of SWIFT waveforms. In each of the remaining examples, we start from the same magnitude excitation spectrum specified in Fig. 16 (top left). A standard SWIFT waveform (Fig. 16, right) may be generated from that magnitude spectrum and a phase spectrum (Fig. 16, bottom left) derived from the linear response relation according to the algorithm described above. However, an undesirable consequence of the phase modulation method designed to reduce the maximum time-domain SWIFT waveform amplitude is temporal discrimination in frequency response (based on the time-shift Fourier theorem) as seen in Fig. 17. The "true" magnitude excitation spectrum (Fig. 17, top, obtained by zero-filling the SWIFT waveform, followed by Fourier transformation) of the *entire* SWIFT waveform closely approximates the originally specified magnitude excitation spectrum (Fig. 16, top left). However, the "true" magnitude excitation spectrum (Fig. 17, middle) computed from just the *first* half of the SWIFT waveform contains only the low-frequency portion of the full excitation spectrum, and "true" magnitude excitation spectrum (Fig. 17, bottom) computed from just the *second* half of

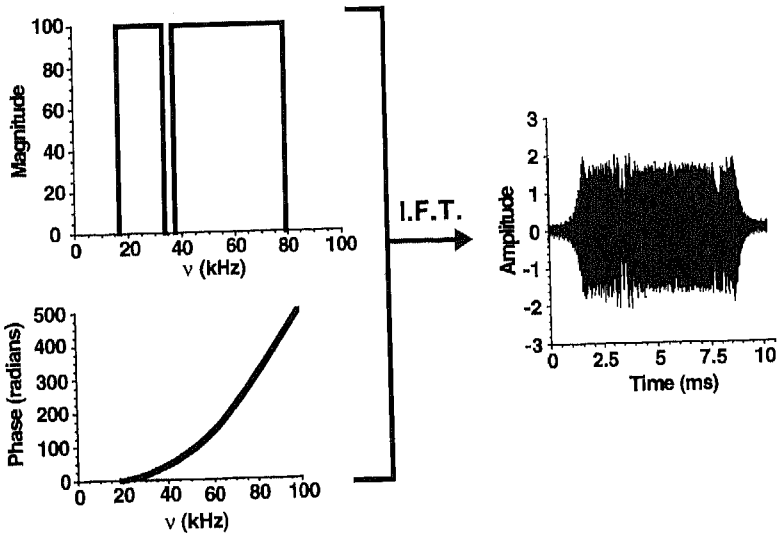

Fig. 16. Top left: Magnitude excitation spectrum (top left) designed for broadband ejection of ions of all but a narrow range of *m/z* values. Bottom left: phase spectrum designed to minimize time-domain SWIFT waveform amplitude as well as reducing the SWIFT waveform amplitude nearly to zero at the beginning and end of the waveform. Right: SWIFT waveform obtained by inverse Fourier transformation of the magnitude/phase spectra at the left of the Figure.

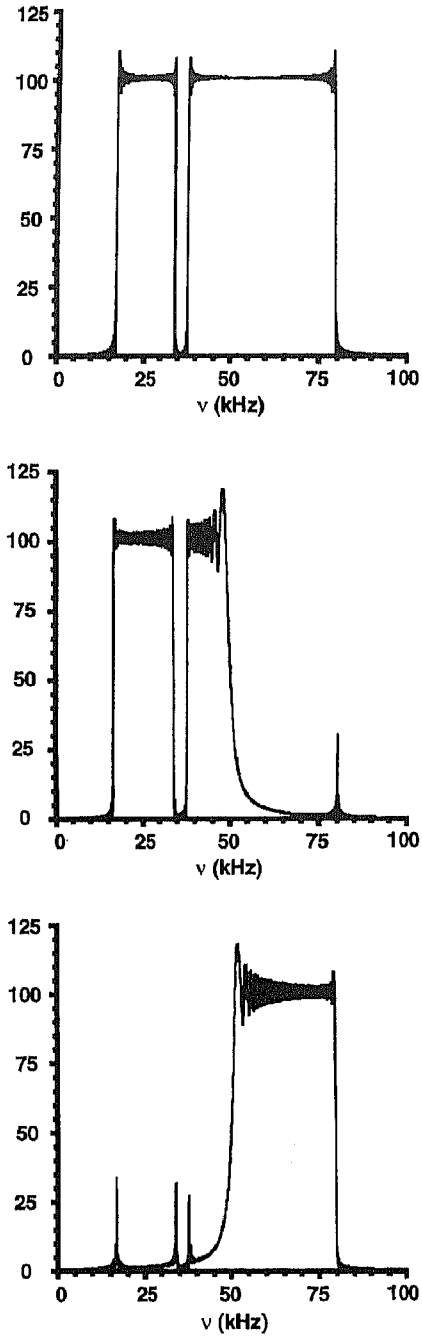

Fig. 17. "True" magnitude excitation spectra obtained by zero-filling the SWIFT waveform of Fig. 16 (right), followed by forward Fourier transformation. Top: Spectrum calculated from the full SWIFT waveform. Middle: Spectrum calculated from just the first half of the SWIFT waveform. Bottom: Spectrum calculated from just the second half of the SWIFT waveform. Note that the low- and high-frequency portions of the spectrum are excited during the first and second halves of the time-domain SWIFT waveform.

the SWIFT waveform contains only the high-frequency portion of the full excitation spectrum. and the second half of the waveform contains the high frequency portion (Fig. 17, middle). Thus, ions of different m/z are excited at different times during the SWIFT waveform. That is not so critical in FT-ICR, for which ion–neutral collisions during the excitation event are usually negligible, but it is undesirable for QIT experiments, for which many collisions may occur during the excitation event. For QIT applications, it is therefore highly desirable to excite ions of all desired m/z values simultaneously.

One obvious solution to the problem is to use a short-duration (and therefore lower-resolution) SWIFT waveform and repeat it many times during the excitation event. In this case, it is important to maintain phase continuity for the various frequency components of the SWIFT waveform. If the phase for a given frequency component differs by 180° from one waveform to the next, then the SWIFT waveform amplitudes will cancel to give zero net excitation at that frequency. Phase continuity (i.e., zero phase difference at any frequency from one SWIFT waveform to the next) may be maintained either by eliminating the delay between consecutive SWIFT waveforms or fixing the delay to be an integral multiple of a single SWIFT waveform duration, because the sinusoidal components of an FFT time-domain waveform always complete their cycles at the end of the waveform. Repeated SWIFT excitation has been used in this way to achieve low-amplitude broadband axialization in FT-ICR MS [74–76]; however, in those examples, an additional time interval was inserted (to allow for collisional damping of cyclotron motion) after each SWIFT excitation waveform, so that phase continuity was not required.

A second approach by Louris and Taylor [77] is equivalent to the use of multiple "foldovers" previously demonstrated for FT-ICR detection [78] in fast Fourier transform (FFT). Consider the inverse FT of a simple rectangular magnitude

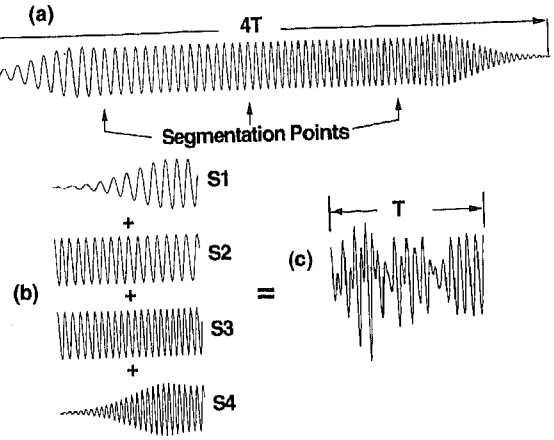

Fig. 18. Analysis of a four times "folded over" SWIFT waveform produced by inverse Fourier transformation of a rectangular ("top-hat") magnitude excitation spectrum and an overmodulated quadratic phase spectrum. The SWIFT waveform (c) can be analyzed as the sum of four segments, S_1 to S_4 (b) of a "virtual" waveform extended to four times the actual time-domain duration (a), so that four frequency components are excited at once (see text).

spectrum and a quadratic phase spectrum (as in Fig. 8, bottom), except that the coefficient of the quadratic term in the phase vs. frequency spectrum corresponds to a bandwidth four times higher than the Nyquist [29] limit. The resulting SWIFT waveform is shown in Fig. 18(c). We may think of that waveform as the sum of four segments, S_1 to S_4, of a "virtual" waveform stretched out to four times the duration of the actual waveform, as shown in Fig. 18(a), (b) (note that segments 2 and 4 are reversed in time before being added to the other two). The decomposition shown in Fig. 18(a), (b) makes it clear that the actual waveform contains four spectral frequency components at any instant during the excitation period. By use of an even higher-amplitude quadratic phase coefficient, even more foldovers can be superimposed, so that more spectral frequencies are excited at once. If the foldover number is sufficiently high, then the SWIFT waveform effectively excites all frequency components simultaneously.

Application of this method to the "notched" magnitude excitation spectrum of Fig. 16 (top left) is shown in Fig. 19. Inverse Fourier transformation of the magnitude excitation spectrum of Fig. 16 (top left) and the "overmodulated"

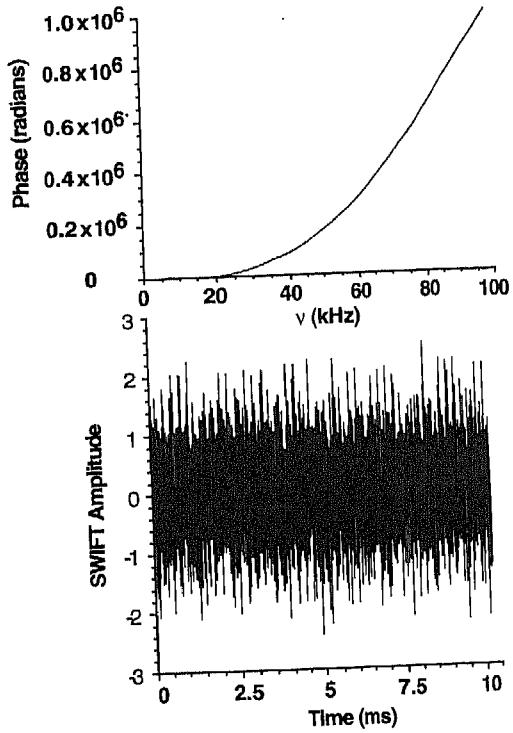

Fig. 19. SWIFT waveform (bottom) produced by inverse Fourier transformation of a "notched" magnitude excitation spectrum (Fig. 16, top left) and a 1000-fold overmodulated phase spectrum (top). In this way, power is distributed more uniformly throughout the SWIFT waveform, and excitation of all frequency components in the spectral bandwidth is near-simultaneous (see text).

quadratic phase spectrum of Fig. 19 (top), calculated from Eq. (3) of Ref. [44] yields the SWIFT waveform shown in Fig. 19 (bottom). The rapid phase variation leads to 1000 Nyquist foldovers in the 10.24 ms of the time-domain waveform. As a result, effectively all of the frequency components (and thus ions of effectively all *m/z* values) are excited simultaneously, as shown by the near-identical "true" magnitude excitation spectra calculated from the entire time-domain SWIFT waveform (Fig. 20, top) or from the first and second halves of the time-domain SWIFT waveform (Fig. 20, middle and bottom). An obvious problem with this approach is the substantial variation in "true" spectral magnitude across the spectral range. Thus, the method would be unsuitable for excitation of ions to a common axial amplitude, but is nevertheless suitable for broadband ion ejection, because the excitation overall amplitude can be set so that the ejection threshold is below the range of magnitude variation. The QIT experiment thus forces one to choose between optimally uniform and selective broadband ion ejection (standard SWIFT phase modulation) and simultaneity of ejection of ions of different *m/z* values (SWIFT phase overmodulation).

A third technique is to distribute the excitation frequency components randomly throughout the time-domain excitation period. Stored-waveform pseudorandom noise was in fact considered in the Tomlinson and Hill's original NMR paper [5] and by Marshall et al. for FT-ICR [79]. However, random phase modulation for SWIFT is usually not employed in FT-ICR due to the extremely nonuniform excitation magnitude vs. frequency profile (unless data from a large number of pseudorandom excitation sequences are combined). For QIT applications, Kelley's so-called "filtered noise field" excitation [72] subjects a time-domain noisy waveform (source not specified in Ref. [72] to a bandpass frequency filter. Ions whose axial secular frequencies fall within the bandpass are not ejected and are therefore isolated by ejection of ions of other *m/z* values.

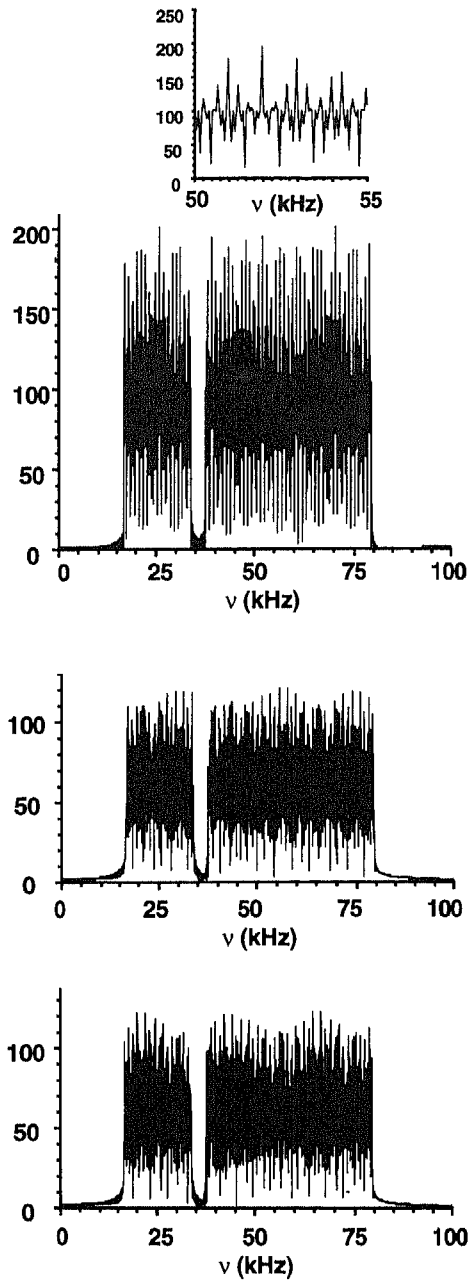

Fig. 20. "True" magnitude excitation spectra obtained by zero-filling the SWIFT waveform of Fig. 19 (bottom), followed by forward Fourier transformation. Top: Spectrum calculated from the full SWIFT waveform. Middle: Spectrum calculated from just the first half of the SWIFT waveform. Bottom: Spectrum calculated from just the second half of the SWIFT waveform. Note that the low- and high-frequency portions of the spectrum are excited essentially equally (but with substantially non-uniform amplitude) during the first and second halves of the time-domain SWIFT waveform.

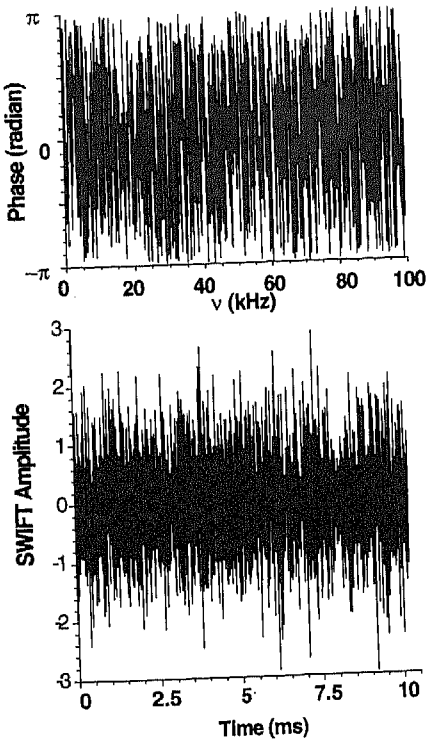

Fig. 21. SWIFT waveform (bottom) produced by inverse Fourier transformation of a "notched" magnitude excitation spectrum (Fig. 16, top left) and a randomly modulated phase spectrum (top). Power is thereby distributed throughout the SWIFT waveform, and excitation of all frequency components in the spectral bandwidth is near-simultaneous (see text).

For the "notched" magnitude excitation spectrum shown in Fig. 16 (top left), a random-phase spectrum can be easily obtained from a software random number generator (Fig. 21, top). Inverse Fourier transformation of the magnitude excitation spectrum of Fig. 16 (top left) and the random phase spectrum yields a noise-like SWIFT waveform (Fig. 21, bottom). The "true" magnitude excitation spectra (Fig. 22, middle and bottom) of the first or second halves of the noisy SWIFT waveform of Fig. 21 (bottom) are similar to each other and to the "true" magnitude excitation spectrum of the entire noisy SWIFT waveform of Fig. 21 (bottom), showing that noise-based excitation can also provide near-simultaneous excitation to all frequency components in a broadband spectrum.

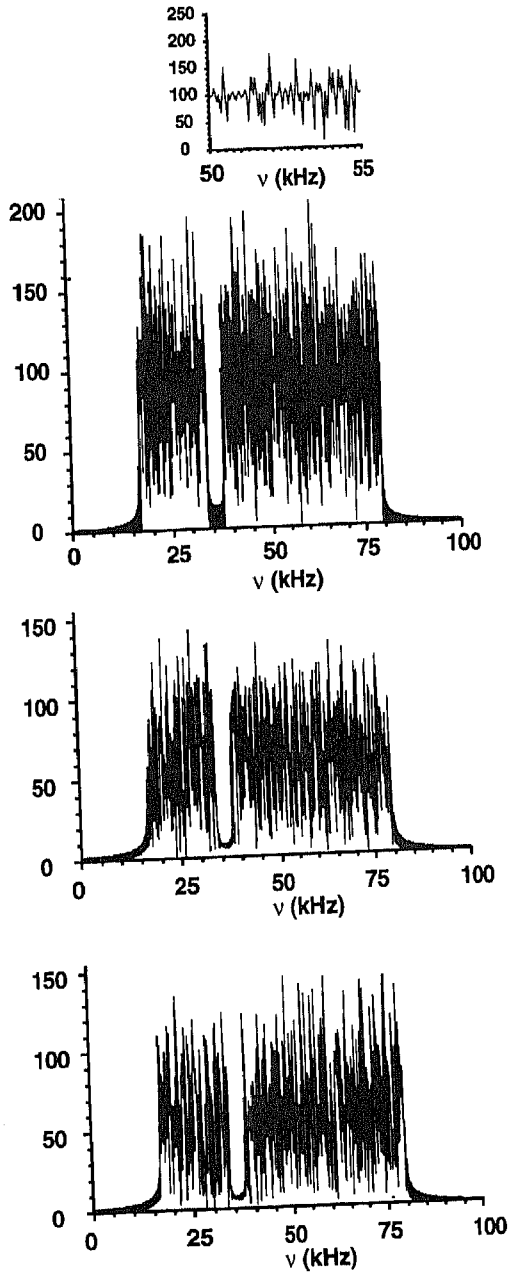

Fig. 22. "True" magnitude excitation spectra obtained by zero-filling the SWIFT waveform of Fig. 21 (bottom), followed by forward Fourier transformation. Top: Spectrum calculated from the full SWIFT waveform. Middle: Spectrum calculated from just the first half of the SWIFT waveform. Bottom: Spectrum calculated from just the second half of the SWIFT waveform. Note that the low- and high-frequency portions of the spectrum are excited essentially equally (but with very non-uniform amplitude) during the first and second halves of the time-domain SWIFT waveform.

9. Conclusion

In summary, stored waveform excitation produced by inverse Fourier transformation of a specified magnitude/phase excitation spectrum offers the most general and versatile means for broadband mass-selective excitation and ejection in Penning (FT-ICR) and Paul (quadrupole) ion trap mass spectrometry. For most purposes, the most desirable SWIFT waveform is that optimized to reduce both the time-domain SWIFT maximum amplitude and the amplitude near the start and end of the SWIFT waveform [44]. It is always desirable to examine the "true" magnitude excitation spectrum, obtained by zero-filling and forward Fourier transforming the SWIFT time-domain waveform, in order to evaluate the trade-off between spectral magnitude uniformity and frequency (mass) selectivity. Apodization of the SWIFT waveform is optimally conducted by smoothing the excitation magnitude spectrum prior to generation of the SWIFT waveform by inverse Fourier transformation. When (as for broadband ejection in a quadrupole ion trap) it is important that ions be excited near-simultaneously over a wide mass range, the phase spectrum (before inverse FT to generate the SWIFT waveform) may be overmodulated or randomly modulated ("filtered noise field"), with the recognition that very substantial non-uniformity in the "true" excitation magnitude spectrum will result. Physical realization of SWIFT excitation is readily available.

Acknowledgements

This work was supported by grants from NSF (CHE-93-22824), N.I.H. (GM-31683), the NSF National High Field FT-ICR Mass Spectrometry Facility (CHE-94-13008), Florida State University, and the National High Magnetic Field Laboratory. The authors thank G. Stafford and J. Syka for helpful discussions and J. Drader for efficient SWIFT implementation on a PC.

References

[1] A.G. Marshall, Acc. Chem. Res., 29 (1996) 307.
[2] R. Freeman, Chem. Rev., 91 (1991) 1397.
[3] P. Pfändler, G. Bodenhausen, J. Rapin, R. Houriet and T. G äumann, Chem. Phys. Lett., 138 (1987) 195.
[4] P. Pfändler, G. Bodenhausen, J. Rapin, M.-E. Walser and T. G äumann, J. Amer. Chem. Soc., 110 (1988) 5625.
[5] B.L. Tomlinson and H.D.W. Hill, J. Chem. Phys., 59 (1973) 1775.
[6] S.A. Lee, C.Q. Jiao, Y. Huang and B.S. Freiser, Rapid Commun. Mass Spectrom., 7 (1993) 819.
[7] A.G. Marshall, T.-C.L. Wang and T.L. Ricca, Chem. Phys. Lett., 105 (1984) 233.
[8] K.A. Boering, J. Rolfe and J.I. Brauman, Int. J. Mass Spectrom. Ion Processes, 117 (1992) 357.
[9] K.A. Boering, J. Rolfe and J.I. Brauman, Rapid Commun. Mass Spectrom., 6 (1992) 303.
[10] J.W. Gauthier, T.R. Trautman and D.B. Jacobson, Anal. Chim. Acta, 246 (1991) 211.
[11] A.G. Marshall, T.-C.L. Wang, L. Chen and T.L. Ricca, Am. Chem. Soc. Symp. Ser., 359 (1987) 21.
[12] L.S. Brown and G. Gabrielse, Rev. Mod. Phys., 58 (1986) 233.
[13] P.B. Grosshans and A.G. Marshall, Anal. Chem., 63 (1991) 2057.
[14] M.B. Comisarow. In: H. Hartmann and K.-P. Wanczek (Ed.), Ion Cyclotron Resonance Spectrometry, Vol. II, Springer-Verlag, Berlin, 1982, p. 484.
[15] P.A. Limbach, P.B. Grosshans and A.G. Marshall, Anal. Chem., 65 (1993)135.
[16] B.S. Freiser. In: T.J. Marks (Ed.), Bonding Energetics in Organometallic Compounds, Vol. 428, Am. Chem. Soc., Washington, DC, 1990, p. 55.
[17] N.M.M. Nibbering, Analyst, 117 (1992) 289.
[18] S. Guan, H.S. Kim, A.G. Marshall, M.C. Wahl, T.D. Wood and X. Xiang, Chem. Rev., 8 (1994) 2161.
[19] S. Guan and A.G. Marshall, Int. J. Mass Spectrom. Ion Processes, 146–147 (1995) 261.
[20] M.B. Comisarow, Int. J. Mass Spectrom. Ion Phys., 37 (1981) 251.
[21] J.D. Jackson, Classical Electrodynamics, Wiley, New York, 1975, 848 pp.
[22] D.W. Mitchell, Int. J. Mass Spectrom. Ion Processes, 107 (1991) 417.
[23] M. Kretzschmar, Phys. Scr., 46 (1992) 544.
[24] R.E. March and R.J. Hughes, Quadrupole Storage Mass Spectrometry, Wiley, New York, 1989, 471 pp.
[25] H.G. Dehmelt, Adv. At. Mol. Phys., 3 (1967) 53.
[26] D. Gerlich, in C.Y. Ng & M. Baer (Ed.), State-Selected and State-to-State Ion–Molecule Reaction Dynamics. Part 1. Experiment, Vol. LXXXII, Wiley, New York, 1992, p. 1.
[27] S. Guan and A.G. Marshall, Anal. Chem., 65 (1993)1288.
[28] G. Gabrielse, Phys. Rev. A, 29 (1984) 462.
[29] A.G. Marshall and F.R. Verdun, Fourier Transforms in NMR, Optical, and Mass Spectrometry: A User's Handbook, Elsevier, Amsterdam, 1990, 460 pp.
[30] S. Guan, J. Am. Soc. Mass Spectrom., 2 (1991) 483.

[31] M.B. Comisarow and A.G. Marshall, Chem. Phys. Lett., 25 (1974) 282.
[32] M.B. Comisarow and A.G. Marshall, Chem. Phys. Lett., 26 (1974) 489.
[33] A.G. Marshall and D.C. Roe, J. Chem. Phys., 73 (1980) 1581.
[34] R.T. McIver, Jr., R.L. Hunter and G. Baykut, Anal. Chem., 61 (1989) 489.
[35] M. Wang and A.G. Marshall, Int. J. Mass Spectrom. Ion Processes, 100 (1990) 323.
[36] M.W. Senko, J.P. Speir and F.W. McLafferty, Anal. Chem., 66 (1994) 2801.
[37] D.E. Goeringer, W.B. Whitten, J.M. Ramsey, S.A. McLuckey and G.L. Glish, Anal. Chem., 64 (1992)1434.
[38] M. Abramowitz and I.A. Stegun (Ed.), Handbook of Mathematical Functions with Formulas, Graphs and Mathematical Tables, U.S. Dept. of Commerce, Washington, DC, 1972.
[39] S. Guan, M.V. Gorshkov, G.M. Alber and A.G. Marshall, Phys. Rev. A, 47 (1993) 2730.
[40] A.G. Marshall, T.-C.L. Wang and T.L. Ricca, J. Amer. Chem. Soc., 107 (1985) 7893.
[41] A.G. Marshall, T.L. Ricca and T.-C.L. Wang, US Patent 4,761,545, issued 2 August, 1988.
[42] L. Chen, T.C.L. Wang, T.L. Ricca and A.G. Marshall, Anal. Chem., 59 (1987) 449.
[43] S. Guan, J. Chem. Phys., 91 (1989) 775.
[44] S. Guan and R.T. McIver, Jr., J. Chem. Phys., 92 (1990) 5841.
[45] S. Goodman and A. Hanna, US Patent 4,945,234, issued 31 July, 1990.
[46] S. Guan, J. Chem. Phys., 93 (1990) 8442.
[47] L. Chen and A.G. Marshall, Rapid Commun. Mass Spectrom., 1 (1987) 39.
[48] S. Guan and P.R. Jones, Rev. Sci. Instrum., 59 (1988) 2573.
[49] S.C. Beu and D.A. Laude, Jr., Anal. Chem., 63 (1991) 2200.
[50] C.D. Hanson, M.E. Castro, E.L. Kerley and D.H. Russell, Anal. Chem., 62 (1990) 1352.
[51] M. Wang and A.G. Marshall, Anal. Chem., 62 (1990) 515.
[52] C.D. Hanson, M.E. Castro, E.L. Kerley and D.H. Russell, Anal. Chem., 62 (1990) 520.
[53] P.B. Grosshans, R. Chen and A.G. Marshall, Int. J. Mass Spectrom. Ion Processes, 139 (1994) 169.
[54] S. Guan, Y. Huang and A.G. Marshall, J. Mass Spectrom., 30 (1995) 1593.
[55] S.L. Mullen and A.G. Marshall, J. Am. Chem. Soc., 110 (1988) 1766.
[56] S. Maruyama, L.R. Anderson and R.E. Smalley, Rev. Sci. Instrum., 61 (1990) 3686.
[57] L. Chen and A.G. Marshall, Int. J. Mass Spectrom. Ion Processes, 79 (1987)115.
[58] T.-C.L. Wang, T.L Ricca and A.G. Marshall, Anal. Chem., 58 (1986) 2935.
[59] E.B. Ledford, Jr., D.L. Rempel and M.L. Gross, Anal. Chem., 56 (1984) 2744.
[60] S. Guan, M.C. Wahl and A.G. Marshall, Anal. Chem., 65 (1993) 3647.
[61] Y. Naito and M. Inoue, J. Mass Spectrom. Soc. Jpn., 42 (1994)1.
[62] L. Pasa-Tolic, Y. Huang, S. Guan, H.S. Kim and A.G. Marshall, J. Mass Spectrom., 30 (1995) 825.
[63] S. Guan, A.G. Marshall and S.E. Scheppele, Anal. Chem., 68 (1996) 46.
[64] S.-P. Chen and M.B. Comisarow, Rapid Commun. Mass Spectrom., 6 (1992) 1.
[65] D.W. Mitchell and R.D. Smith, Phys. Rev. E, 52 (1995) 4366.
[66] A.J. Peurrung and R.T. Kouzes, Int. J. Mass Spectrom. Ion Processes, 145 (1995) 139.
[67] S. Haebel and T. Gäumann, Int. J. Mass Spectrom. Ion Processes, 144 (1995) 139.
[68] S. Haebel, M.-E. Walser and T. Gäumann, Int. J. Mass Spectrom. Ion Processes, 151 (1995) 97.
[69] C.W. Ross, III, S. Guan, P.B. Grosshans, T.L. Ricca and A.G. Marshall, J. Am. Chem. Soc., 115 (1993) 7854.
[70] M.H. Soni and R.G. Cooks, Anal. Chem., 66 (1994) 2488.
[71] P.E. Kelley, US Patent 5,134,286, issued 28 July, 1992.
[72] D.E. Goeringer, K.G. Asano, S.A. McLuckey, D. Hoekman and S.W. Stiller, Anal. Chem., 66 (1994) 313.
[73] S. Guan, M.C. Wahl and A.G. Marshall, J. Chem. Phys., 100 (1994) 6137.
[74] J.A. Marto, S. Guan and A.G. Marshall, Rapid Commun. Mass Spectrom., 8 (1994) 615.
[75] Y. Huang, L. Pasa-Tolic, S. Guan and A.G. Marshall, Anal. Chem., 66 (1994) 4385.
[76] J.N. Louris and D.M. Taylor, US Patent 5,324,939, issued 28 June, 1994.
[77] M. Wang and A.G. Marshall, Anal. Chem., 60 (1988) 341.
[78] A.G. Marshall, T.-C.L. Wang and T.L. Ricca, Chem. Phys. Lett., 108 (1984) 63.